

Velocity reassignment echoes in proteins

Dong Xu and Klaus Schulten

Department of Physics and Beckman Institute, University of Illinois at Urbana–Champaign, Urbana, Illinois 61801

(Received 10 January 1995; accepted 24 April 1995)

A new echo phenomenon in proteins, a generalization of so-called temperature quench echoes, is introduced and shown to reveal, through molecular dynamics simulations, periodic motions (normal modes) in proteins with phase coherence times of about one picosecond. The echoes are induced through reassignments of Cartesian velocities to protein atoms at times $t=0$ and $t=\tau$ ($0<\tau\leq 1$ ps) and appear as two sharp (widths of about 5 fs) features in the kinetic and potential energy at $t=3\pi/2$ and $t=2\tau$. The velocities, assigned at $t=0$ and at $t=\tau$ to each atom, need to be correlated, but can otherwise be random. The echo at $3\pi/2$ can be induced without any change in the temperature of the protein. Skeletal motions involving angular and stretch motions contribute principally to the echo effect. Electrostatic interactions do not affect the echoes. The echoes in the temperature are described, in the framework of the harmonic approximation, in terms of the equilibrium temperature–temperature correlation function. The velocity reassignments induce the echoes through the generation of phase coherence of protein modes. Phase relaxation due to anharmonic interactions, lead to a dependence of the echo depths on the time interval τ between velocity replacements which can be accounted for by phase diffusion or by Langevin oscillators. The echo effect can provide a sensitive probe for the study of non-diffusive energy transport in proteins. © 1995 American Institute of Physics.

I. INTRODUCTION

Motions in proteins have been studied by observation and by molecular dynamics simulation for many years, but are still only poorly understood. In case of solids and small molecules our understanding of characteristic motions, comparably, is in a vastly better state, owing much to investigations of periodic motions in these systems.^{1,2} Following this example researchers have studied normal modes also in proteins. Normal mode analysis has been used, for example, to describe the fluctuations and display concerted motions of proteins.^{3–9} Normal modes have been applied to model slow motions between protein domains, for example, the hinge-bending motion of lysozyme.^{10,11}

An experimental access to normal modes in proteins is provided by incoherent neutron scattering and observations of density of states were found in agreement with simulations.^{12,13} Many observations have focussed on oxygen carrying heme proteins. Inelastic neutron scattering spectra in Ref. 14 have resolved the density of states of the modes of myoglobin in the low-frequency regime. Site-selective fluorescence spectroscopy of Zn-substituted myoglobin has obtained this density without the use of model shape functions.¹⁵ Recent photoacoustic studies of proteins in D₂O using ps IR spectroscopy have revealed two forms of energy transport, a classical diffusive path and a faster avenue, likely involving concerted protein motions.¹⁶ Resonance Raman spectroscopy using ps laser pulses have been interpreted through relaxation of protein normal modes, assigning a dephasing time of 500 fs.¹⁷ A recent review of related studies and of observations of protein dynamics using phase grating spectroscopy is found in Ref. 18. Due to these exciting investigations protein normal modes promise to command the interest of spectroscopists for years to come.

Protein normal modes hold a particular fascination also for theoretical protein science since they are thought to pro-

vide suitable basis vectors for long-time integration methods^{19,20} and can serve to simplify molecular dynamics simulations through constraints to low-frequency modes.²¹ Normal modes also provide a classification scheme for proteins dividing forces into harmonic and anharmonic.^{22,23} The significant anharmonic contributions of force fields in proteins, such as torsional potentials, electrostatic and van der Waals interactions, call into question the existence of protein normal modes and even the existence of periodic or coherent motions. The widely adopted method to obtain normal modes for proteins is to calculate the second derivative (Hessian) matrix of the potential energy with respect to Cartesian coordinates or with respect to internal coordinates, and to diagonalize this matrix.³ Due to anharmonic effects, normal modes defined through this method are not unique, but rather depend on the conformation of a protein. One would like to know how these modes, which are defined strictly only at $T=0$, manifest themselves at higher temperatures.

Beyond a description through the Hessian matrix, there are few other tools to describe normal modes in proteins. A welcome exception is the temperature quench echo (TQE) phenomenon. The TQE was first observed in simulations of disordered solids by Grest *et al.*^{24–27} and had been applied recently to the protein bovine pancreatic trypsin inhibitor (BPTI) by Becker and Karplus.²⁸ The basic idea of the TQE can be summarized as follows: A molecular dynamics simulation of a system at a certain temperature is halted twice, at times $t=0$ and $t=\tau$, each time the simulation is continued with the same positions, but with all atomic velocities replaced by zero velocities. This procedure is referred to as a double quench. After this quench, at time 2τ , one observes a dip in the temperature of the system defined through the total kinetic energy $E_k(t)$:

$$T(t) = \frac{2}{3k_B N} E_k(t), \quad (1)$$

$$E_k(t) = \sum_i \frac{1}{2} m_i \mathbf{v}_i^2(t), \quad (2)$$

where N denotes the number of atoms. In microcanonical simulations holds $E_k(t) + V(t) = E = \text{constant}$, such that the TQE can also be observed through a bump in the potential energy $V(t)$, an obvious possibility not considered before.

The TQE arises from coherent harmonic motions of a protein induced through the double quench, setting the protein temperature twice to zero values.^{28,29} Generalizations of the double quench procedure involved cool–heat–cool sequences instead of a cool–cool sequence.²⁸ All the methods employed involved a significant change of temperature and, hence, a major perturbation. For example, double quenches reduce a protein's temperature to a quarter of the initial temperature T_0 , e.g., from 300 K to 75 K.

In this paper, we will introduce an echo phenomenon which generalizes the TQE in a seemingly straightforward way: rather than reassigning twice, i.e., at times $t=0$ and $t=\tau$, zero velocities to a protein's atoms, one assigns velocities from two random, but correlated sets of velocities. In general, one obtains through such procedure echoes at $3\tau/2$, along with the conventional 2τ echoes. We will refer to this echo as the velocity reassignment echo (VRE). In case that the VRE procedure uses at $t=0$ and at $t=\tau$ identical sets of velocities obeying a Maxwell distribution for temperature T_0 , where T_0 is the equilibrium temperature of the starting structure, the echo at $t=2\tau$ disappears, but the echo at $t=3\tau/2$ remains. Such procedure avoids any temperature change in the system.

The VRE can be exploited to yield further insight into normal modes of proteins. One possibility is to study the effects of anharmonic interactions which, due to phase relaxation, induce a dependence of the echo depth on the time interval τ . Another possibility is to monitor the echo through $V(t)$ rather than $E_k(t)$ so that one can determine which potential energy terms, e.g., torsional or stretch, participate significantly in the echo and, thereby, identify the types of motions which give rise to quasi-harmonic protein motions.

In Section II of this paper the molecular dynamics simulation methods used are briefly presented. In Section III the VRE simulation procedure is described and exemplary simulation results are discussed. Section IV focuses on simulation results for $V(t)$ -echoes and analyses how different types of potential energies participate in these echoes. In Section V the theory of the VRE is derived in the harmonic approximation; echoes are expressed in terms of temperature-temperature correlation functions and the results compared with simulation data. In Section VI the phase coherence induced by velocity reassignments is demonstrated and mathematically characterized. Section VII introduces a simple phase relaxation model which accounts phenomenologically for the τ - and temperature dependence of the echo depth. Section VIII presents a model of Langevin oscillators which provides an alternative description of the echo depth. In Section IX we discuss the main implications of this paper and suggest future studies.

II. METHODS

All simulations described in this paper were carried out for the protein BPTI starting from the 1.5 Å resolution x-ray structure,³⁰ with 58 amino acids and 898 explicit atoms. The simulations employed the molecular dynamics package MD/PMD developed in our group together with the fast multipole approximation (FMA) to evaluate long range electrostatic forces.^{31,32} The CHARMM all-atom potential energy function (parmallh3x.pro) and partial charge distribution (topallh6x.pro) were used.³³ The dielectric constant assumed was $\epsilon=1$ and the time step was chosen as 0.5 fs. Neither distance cutoff for non-bonded interaction nor the explicit hydrogen bonding energy function was employed. The equilibrated structures at a certain temperature T_0 were achieved through coupling to a heat bath at T_0 by rescaling velocities through³⁴

$$v_i^{\text{new}} = v_i^{\text{old}} \sqrt{1 - \lambda + \lambda T_0/T}, \quad (3)$$

where $\lambda=0.01$ and where T is the temperature defined in Eq. (1). During the simulations of velocity reassignments, including 5 ps before the first velocity reassignments, no coupling to a heat bath was applied.

In order to investigate echoes in BPTI without any electrostatic interactions (c.f. Fig. 4), we employed the program X-PLOR³⁵ with the same conditions as described above, except that the electrostatic energy term was turned off during the simulations. For this purpose, we started from a 300 K structure for full potential energies and equilibrated this system without electrostatic forces, coupling to a heat bath at 300 K.

III. SIMULATION OF VELOCITY REASSIGNMENT ECHOES

In this section, we will describe the simulation procedure for the velocity reassignment echo (VRE). We introduce, by way of the example presented in Figure 1(a) the simulation procedures which produce the VRE. In this case BPTI was equilibrated at $T_0=200$ K. The simulation continued without velocity rescaling for 5 ps and was then halted at time $t=0$. A set of Cartesian velocities

$$\mathcal{V}^{(1)} = \{v_1^{(1)}, v_2^{(1)}, v_3^{(1)}, \dots, v_{3N}^{(1)}\} \quad (4)$$

was chosen, each velocity component $v_i^{(1)}$ being generated randomly according to the Maxwell distribution at temperature $T_1=40$ K, i.e., according to

$$f(v_i^{(1)}) = \sqrt{\frac{m_i}{2\pi k_B T_1}} \exp\left[-\frac{m_i (v_i^{(1)})^2}{2k_B T_1}\right]. \quad (5)$$

The $3N$ elements of $\mathcal{V}^{(1)}$ in Eq. (4) were assigned as the new velocities in the x, y, z -directions of the N protein atoms. The simulation was resumed and after $\tau=100$ fs was halted again. Then random velocities of the set

$$\mathcal{V}^{(2)} = \{v_1^{(2)}, v_2^{(2)}, v_3^{(2)}, \dots, v_{3N}^{(2)}\} \quad (6)$$

were assigned to the atoms. This second set of velocities was chosen strongly correlated with the velocities in Eq. (4), using

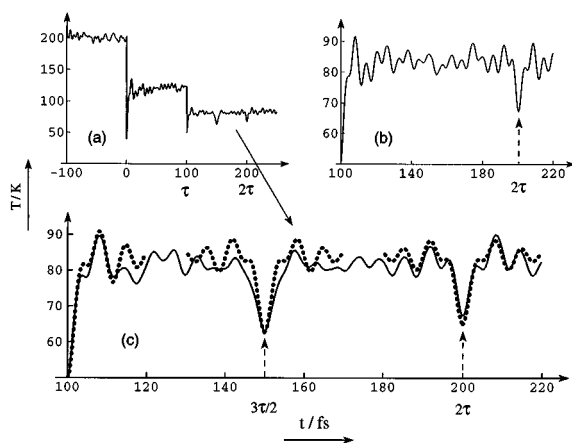


FIG. 1. (a) Procedure of velocity reassignments and resulting temperature changes: Starting from an equilibrated structure at $T_0=200$ K, one reassigns velocities at $t=0$ and again at $t=\tau$ using random velocities corresponding to $T_1=40$ K for a set (4), and to $T_2=50$ K for a set (6), respectively ($\tau=100$ fs). The difference between two sets of velocities assigned at $t=0$ and $t=100$ fs is a constant factor, i.e., $\lambda=\sqrt{5}/2$ [cf. Eq. (7)]; (b) temperature response at $t>\tau$ with the same conditions as in (a), except that two sets of velocities assigned at $t=0$ and $t=100$ fs, i.e., (4) and (6), are uncorrelated; (c) enlargement of (a) (solid line) and comparison with (44) for $\lambda_1=1/\sqrt{5}$ and $\lambda_2=1/2$ (dotted line).

$$\mathcal{V}^{(2)} = \{\lambda v_1^{(1)}, \lambda v_2^{(1)}, \lambda v_3^{(1)}, \dots, \lambda v_{3N}^{(1)}\} = \lambda \mathcal{V}^{(1)}. \quad (7)$$

As indicated, the second set of velocities is related to set (4) through a constant factor λ . One can readily show that the elements in $\mathcal{V}^{(2)}$ satisfy the Maxwell distribution (5) for a temperature $T_2=\lambda^2 T_1$. In case of the simulation in Fig. 1, we chose $\lambda=\sqrt{5}/2$ such that $T_2=50$ K. The simulation was again resumed and the kinetic temperature $T(t)$, evaluated according to Eqs. (1) and (2), was monitored. Figure 1(a) shows the trace of $T(t)$ and demonstrates the occurrence of an echo at $t=150$ fs and one at $t=200$ fs, i.e., at $t=3\pi/2$ and at $t=2\tau$.

An essential element in the procedure for velocity reassignment echoes is a significant correlation of the two sets of velocities employed in the two reassignments, i.e., the correlation of the sets (4) and (6). To demonstrate the necessity for such correlation we have carried out two velocity reassignments, a first reassignment at $t=0$ like in case of Fig. 1(a), and a second reassignment at $t=\tau=100$ fs with a set (6) chosen uncorrelated with Eq. (4), i.e., the elements of the set (6) were randomly selected according to a Maxwell distribution at temperature 50 K. Figure 1(b) presents the trace of $T(t)$ after the two velocity reassignments. Comparison with Figure 1(a) shows that the echo at $t=3\pi/2=150$ fs disappears, whereas the echo at $t=2\tau=200$ fs remains. This result indicates that the echo at $t=2\tau$ is connected with a change in overall temperature, whereas the echo at $t=3\pi/2$ is connected with the correlation between the sets of reassignment velocities (4) and (6).

To test this hypothesis we have also adopted a procedure in which a temperature change is avoided, but a strong correlation is retained. Such procedure reassigns at $t=0$ and $t=\tau$ the same set of random velocities corresponding to the equilibrium temperature T_0 , i.e., one employs the same pro-

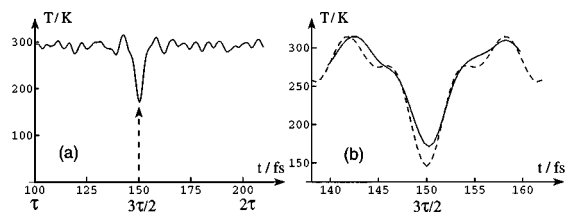


FIG. 2. (a) Velocity reassignments at $t=0$ and $t=\tau$ for $\lambda=1$ in (7), with $T_0=T_1=T_2=300$ K ($\tau=100$ fs); (b) enlargement of (a) (solid line) and comparison with the temperature response expressed according to (48) (dashed line).

cedure as in case of Figure 1(a), except that one chooses for the sets (4) and (6) temperatures $T_1=T_2=T_0$. Figure 2(a) presents the trace of $T(t)$ after such velocity reassignments. One notes, indeed, that the echo at $t=2\tau$ disappears and only the echo at $t=3\pi/2$ remains. This type of echo is altogether unrelated to the TQE. As the trace of $T(t)$ in Fig. 2(a) shows this echo avoids completely a change of temperature, i.e., it involves a gentle perturbation. We will refer to this phenomenon as the *constant temperature velocity reassignment echo* (CVRE).

IV. POTENTIAL ENERGY ECHOES

Due to conservation of total energy the velocity reassignment echoes can be monitored also as a bump in the total potential energy $V(t)$ of the system. On first sight this is unappealing since the total potential energy is more difficult to evaluate than the kinetic energy. However, this approach permits one to dissect the $V(t)$ -echo into its various contributions, e.g., contributions from bond, van der Waals and electrostatic energies; such analysis allows one then to conclude which type of motions participate significantly in the normal modes underlying the echo effect.

The potential energy of a protein, as employed in molecular dynamics simulations, is partitioned into so-called bond, angle, dihedral, improper, electrostatic and van der Waals contributions:^{33,36}

$$V(t) = V_{\text{bond}}(t) + V_{\text{angle}}(t) + V_{\text{dihc}}(t) + V_{\text{impr}}(t) + V_{\text{elec}}(t) + V_{\text{vdw}}(t). \quad (8)$$

The bond energy and angle energy are described by quadratic functions

$$V_{\text{bond}} = \frac{1}{2} \sum_{\text{bonds}} k_b (|\mathbf{r}| - r_0)^2; \quad (9)$$

$$V_{\text{angle}} = \frac{1}{2} \sum_{\text{angles}} k_a (\theta - \theta_0)^2.$$

These terms contribute the strongest forces in a protein and, accordingly, one expects that these energy terms dominate the $V(t)$ -echo. The dihedral and improper terms can be described in a common functional form

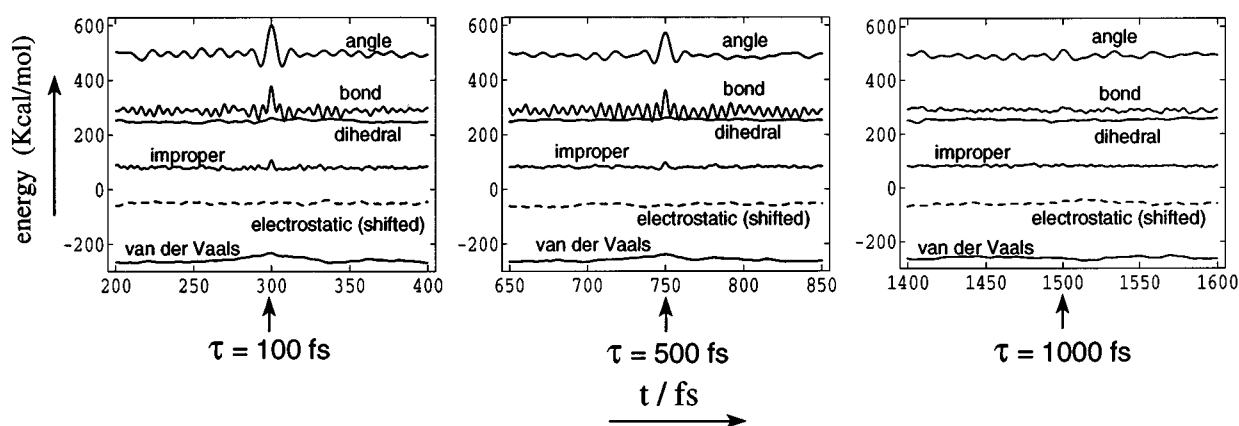


FIG. 3. Potential energy response in case of CVRE at $T_0=300$ K for different τ 's (electrostatic energy is shifted by +2200 kcal/mol). The energy traces are averaged over five independent simulations. The positions of the echoes are marked by arrows.

$$V_{\text{torsion}} = \begin{cases} \sum_{\text{torsion}} k_{\phi} [1 + \cos(n\phi + \phi_0)] & (n=1,2,3,\dots) \\ \sum_{\text{torsion}} k_{\phi} (\phi - \phi_0)^2. & \end{cases} \quad (10)$$

The electrostatic and van der Waals energies, the so-called non-bonded energy contributions, are described by the functions

$$V_{\text{elec}} = \sum_{\text{pairs}} \frac{q_1 q_2}{\epsilon r}; \quad V_{\text{vdw}} = \sum_{\text{pairs}} \left(\frac{A}{r^{12}} - \frac{B}{r^6} \right). \quad (11)$$

In this section we consider the echo resulting from a CVRE procedure at $T_0=300$ K for time intervals $\tau=200,400,1000$ fs. Figure 3 presents the contributions of the potential energy terms in Eq. (8) to the respective $V(t)$ -echoes. The results in Fig. 3 demonstrate that $V_{\text{angle}}(t)$ exhibits the largest contribution to the echo. The second largest contribution arises from $V_{\text{bond}}(t)$. The remaining potential energy terms contribute insignificantly, in particular, the electrostatic energy term shows no discernible contribution. One can interpret the results in Fig. 3 as a proof that the normal modes participating in the echoes are skeletal motions involving bending vibrations (which affect bond angles) and involving, to a lesser degree, stretch vibrations.

The indifference of the electrostatic energy to the echo effect is further demonstrated by a simulation, in which all the electrostatic forces in BPTI were turned off. We demonstrate below (see Sections VII, VIII) that the depth of the echo is governed by anharmonic interactions which lead to vibrational dephasing. One might expect that the distinctly anharmonic electrostatic interactions would affect the depth of the echo; surprisingly, the results presented in Fig. 4 show that the echo depth is not affected by the electrostatic interactions. We explain this indifference of electrostatic interactions to the echoes as follows: consider two charges separated by a distance r_0 in an equilibrated protein; if both charges involve harmonic motions with amplitudes δr , the energy perturbation of the electrostatic energy due to the harmonic motions is of the order of $\delta r/r_0$; however, in

folded proteins δr is much smaller than r_0 and, hence, the electrostatic interactions do not influence protein modes significantly.

V. THEORY OF VELOCITY REASSIGNMENT ECHOES

In this section we provide a formal description of the VRE and compare its predictions with simulation results. Such description can be obtained by expressing the signal $T(t)$ through a suitable ensemble average of the kinetic energy $E_k(t)$ as it results after two velocity reassignments. An analytical treatment is possible only in the framework of the harmonic approximation. In this framework one can express the signal $T(t)$ in terms of the temperatures T_0 , T_1 and T_2 introduced above and in terms of the normalized temperature-temperature correlation function

$$C_{T,T}(t) = \frac{\langle T(t)T(0) \rangle - \langle T(t) \rangle^2}{[\langle T(t) \rangle^2] - \langle T(t) \rangle^2}. \quad (12)$$

This function can be determined from simulations of equilibrated proteins before any velocity reassignment is applied.

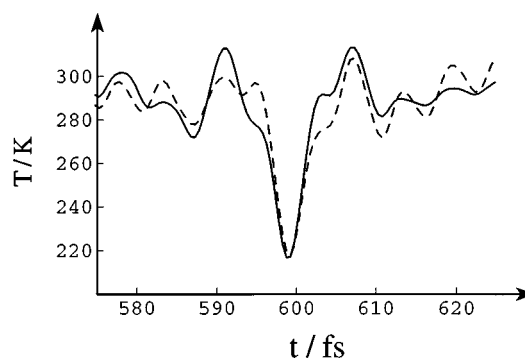


FIG. 4. Comparison of CVREs at $\tau=400$ fs and $T_0=300$ K for BPTI with CHARMM³³ partial atomic charges (dashed line) and with vanishing atomic charges (solid line).

A. Three stages of normal mode dynamics

In the harmonic approximation, for a protein with N atoms, there are $3N-6$ different internal normal modes. Six degrees of freedom, which describe overall translation and rotation, are not counted as normal modes. We denote the frequency of the α th mode by ω_α , the corresponding effective mass by m_α , and the associated vibrational coordinate by x_α , where $\alpha=1,2,\dots,3N-6$. For the purpose of our derivation, we divide the dynamics governing the velocity reassignments and resulting echoes into three stages: (0) before the first reassignment, (1) between the first and the second reassignment, and (2) after the second reassignment.

Normal modes imply concerted motions in which many protein atoms participate. The modes are described through a linear transformation from atomic coordinates X_j , $j=1, 2,\dots,3N$ to normal mode coordinates x_α , $\alpha=1,2,\dots,3N-6$:

$$x_\alpha = \sum_{j=1}^{3N} S_{\alpha j}(t) X_j. \quad (13)$$

We have indicated through a time-dependence of the transformation matrix $\mathbf{S}(t)$ that the normal modes in a non-harmonic system, like a protein, are not invariant in time. In fact, one expects that the modes in proteins vary in time and, consequently, that the matrix $\mathbf{S}(t)$ experiences significant changes while a protein moves across conformational substates.³⁷ Since the evolution of the transformation matrix $\mathbf{S}(t)$ is unknown it is, strictly speaking, impossible to carry the velocity correlation expressed in Eq. (7) over to a normal mode analysis. In fact, defining the normal mode velocities at $t=0$

$$u_\alpha^{(1)} = \sum_{j=1}^{3N} S_{\alpha j}(0) v_j^{(1)} \quad (14)$$

and at $t=\tau$,

$$\tilde{u}_\alpha^{(2)} = \sum_{j=1}^{3N} S_{\alpha j}(\tau) v_j^{(2)} \quad (15)$$

the sets of velocities, which should be assigned to the normal modes, are

$$\mathcal{U}^{(1)} = \{u_1^{(1)}, u_2^{(1)}, u_3^{(1)}, \dots, u_{3N-6}^{(1)}\}. \quad (16)$$

and

$$\tilde{\mathcal{U}}^{(2)} = \{\tilde{u}_1^{(2)}, \tilde{u}_2^{(2)}, \tilde{u}_3^{(2)}, \dots, \tilde{u}_{3N-6}^{(2)}\}, \quad (17)$$

corresponding to the velocity sets (4) and (6), respectively. However, the lack of knowledge of $\mathbf{S}(\tau)$ forces us to rather employ, at time $t=\tau$, the velocities transformed by $\mathbf{S}(0)$

$$u_\alpha^{(2)} = \sum_{j=1}^{3N} S_{\alpha j}(0) v_j^{(2)} \quad (18)$$

and, hence, the set

$$\mathcal{U}^{(2)} = \{u_1^{(2)}, u_2^{(2)}, u_3^{(2)}, \dots, u_{3N-6}^{(2)}\} \quad (19)$$

can be written, according to Eq. (7),

$$\mathcal{U}^{(2)} = \{\lambda u_1^{(1)}, \lambda u_2^{(1)}, \lambda u_3^{(1)}, \dots, \lambda u_{3N-6}^{(1)}\} = \lambda \mathcal{U}^{(1)}. \quad (20)$$

For the statistical characteristics of the velocities $u_\alpha^{(1)}$ and $u_\alpha^{(2)}$ and their correlation the transformation $\mathbf{S}(0)$ is immaterial. Since the reassigned velocities are characterized only through their average properties the transformation matrix $\mathbf{S}(0)$ is not required; one can apply the statistical characteristics directly to $u_\alpha^{(1)}$ and $u_\alpha^{(2)}$ without knowing the Cartesian velocities $v_j^{(1)}$ and $v_j^{(2)}$. However, the replacement $\mathbf{S}(\tau) \rightarrow \mathbf{S}(0)$ implies an error for the correlation of velocities, as described, for example, by Eq. (7). The correlation of two velocities $u_\alpha^{(1)}$ and $\tilde{u}_\alpha^{(2)}$ can be written, using Eq. (20),

$$\langle u_\alpha^{(1)} \tilde{u}_\alpha^{(2)} \rangle_u = g_\alpha(\tau, T) \langle u_\alpha^{(1)} u_\alpha^{(2)} \rangle_u = g_\alpha(\tau, T) \lambda \langle [u_\alpha^{(1)}]^2 \rangle_u. \quad (21)$$

Here $g_\alpha(\tau, T)$ is a factor accounting for the difference between $\mathbf{S}(\tau)$ and $\mathbf{S}(0)$ and is a function of the time interval τ and temperature T . In the harmonic case, which is assumed in this Section, $g_\alpha(\tau, T) = 1$. But for proteins, due to anharmonic effects, one expects $0 < g_\alpha(\tau, T) < 1$, $g_\alpha(\tau, T)$ deviating more from unity, the longer τ . We will argue in Section VII that the deviation of g_α from 1 affects solely the $\frac{3}{2}\tau$ -echo, and not the 2τ -echo.

1. Before the first reassignment

During this stage, the position of the α th normal mode at $t < 0$ can be expressed as

$$x_\alpha^{(0)}(t) = A_\alpha \cos(\omega_\alpha t + \theta_\alpha), \quad (22)$$

where A_α denotes the amplitude of the mode which is related to the mode's total energy and where θ_α denotes the phase of the mode which is related to the initial values of the mode's position and velocity

$$\frac{dx_\alpha^{(0)}(t)}{dt} = -A_\alpha \omega_\alpha \sin(\omega_\alpha t + \theta_\alpha). \quad (23)$$

For a thermally equilibrated ensemble the amplitudes A_α are randomly distributed, obeying the Rayleigh distribution³⁸

$$P(A_\alpha) = \frac{m_\alpha \omega_\alpha^2 A_\alpha}{k_B T_0} \exp\left(-\frac{m_\alpha \omega_\alpha^2 A_\alpha^2}{2k_B T_0}\right). \quad (24)$$

The phases θ_α , likewise, are random; they are evenly distributed in the interval $[0, 2\pi]$. Obviously, averaging over the phases yields

$$\langle \cos(n\theta) \rangle_\theta = 0; \quad n = 1, 2, 3, \dots \quad (25)$$

The temperature correlation function $C_{T,T}(t)$ defined in Eq. (12), can be expressed through averages over the kinetic energy of the system. In Ref. 29 it has been derived:

$$C_{T,T}(t) = \langle \cos(2\omega_\alpha t) \rangle_\alpha. \quad (26)$$

Here $\langle \dots \rangle_\alpha$ denotes an average over all the normal modes, i.e.,

$$\langle f(\omega_\alpha) \rangle_\alpha = \frac{1}{3N-6} \sum_\alpha f(\omega_\alpha) = \int_0^\infty d\omega D(\omega) f(\omega), \quad (27)$$

where $D(\omega)$ represents the so-called density of states.

Instead of evaluating $C_{T,T}(t)$ using Eqs. (26) and (27), one can determine $C_{T,T}(t)$, according to its definition (12), from molecular dynamics simulations which do not involve

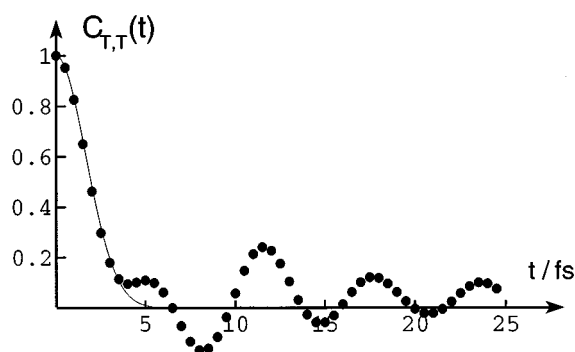


FIG. 5. Temperature correlation function; the dots represent $C_{T,T}(t)$ from a 5 ps simulation at $T_0=297.86$ K, evaluated according to Eq. (12); the continuous line shows expression (28).

the harmonic approximation. In the present study the evaluation of $C_{T,T}(t)$ was based on a 5 ps simulation without coupling to any heat bath.²⁹ The resulting correlation function is presented in Fig. 5. Following Ref. 39 one can crudely match $C_{T,T}(t)$ to the function

$$C_{T,T}(t) \approx \exp\left[-\left(\frac{t}{\tau_0}\right)^2\right], \quad \tau_0 = 2.35 \text{ fs}, \quad (28)$$

where the decay time τ_0 had been determined through a least-square fit. This approximation, also shown in Fig. 5, introduces a natural time scale τ_0 , which will be used repeatedly. In particular, we will use

$$C_{T,T}(t) \approx 0 \quad (\tau \gg \tau_0). \quad (29)$$

2. After the first reassignment and before the second one

After the first reassignment and before the second one, i.e., for $0 \leq t < \tau$, the position for the α th normal mode can be expressed as

$$x_\alpha^{(1)}(t) = A_\alpha^{(1)} \cos(\omega_\alpha t + \theta_\alpha^{(1)}). \quad (30)$$

This expression must be matched, at $t=0$, to the positions $x_\alpha^{(1)}(0)$ predicted by expression (22), i.e., it must hold

$$A_\alpha^{(1)} \cos \theta_\alpha^{(1)} = A_\alpha \cos \theta_\alpha. \quad (31)$$

At $t=0$, the velocities for all modes α are randomly assigned elements of $\mathcal{V}^{(1)}$ [see Eq. (16)]. This implies the second condition

$$\frac{dx_\alpha^{(1)}(0)}{dt} = -A_\alpha^{(1)} \omega_\alpha \sin \theta_\alpha^{(1)} = u_\alpha^{(1)}. \quad (32)$$

From Eqs. (31) and (32) one can determine the quantities $A_\alpha^{(1)}$ and $\theta_\alpha^{(1)}$ and, hence, describe the motion for $t \geq 0$ according to (30).

3. After the second reassignment

After the second reassignment, i.e., at $t \geq \tau$, the position of the α th normal mode can be expressed as

$$x_\alpha^{(2)}(t) = A_\alpha^{(2)} \cos[\omega_\alpha(t - \tau) + \theta_\alpha^{(2)}]. \quad (33)$$

This expression must be matched, at $t=\tau$, to the positions $x_\alpha^{(1)}(\tau)$ given by Eq. (30), i.e., it must hold in analogy to Eq. (31),

$$A_\alpha^{(2)} \cos \theta_\alpha^{(2)} = A_\alpha^{(1)} \cos(\omega_\alpha \tau + \theta_\alpha^{(1)}). \quad (34)$$

At $t=\tau$ one reassigns the random velocities in $\mathcal{V}^{(2)}$ [see Eq. (19)] with $\lambda = \sqrt{T_2/T_1}$. Employing the condition Eq. (20) one obtains, in analogy to Eq. (32),

$$\frac{dx_\alpha^{(2)}(\tau)}{dt} = -A_\alpha^{(2)} \omega_\alpha \sin \theta_\alpha^{(2)} = \lambda u_\alpha^{(1)}. \quad (35)$$

Defining

$$u_\alpha = u_\alpha^{(1)} / \lambda_1, \quad (36)$$

where $\lambda_1 = \sqrt{T_1/T_0}$, one can restate Eq. (35),

$$-A_\alpha^{(2)} \omega_\alpha \sin \theta_\alpha^{(2)} = \lambda_2 u_\alpha, \quad (37)$$

where $\lambda_2 = \lambda \lambda_1 = \sqrt{T_2/T_0}$. We note that the velocities u_α satisfy

$$\langle m_\alpha u_\alpha^2 \rangle_u = k_B T_0. \quad (38)$$

Equations (34) and (37) allow one to determine $A_\alpha^{(2)}$ and $\theta_\alpha^{(2)}$ and to describe the motion for $t \geq \tau$ according to Eq. (33).

B. Expression for the temperature echoes

We are now in a position to determine the kinetic energy and, thereby, the temperature after the velocity reassignments. The resulting kinetic energy is

$$E_k^{(2)}(t) = \sum_\alpha \frac{1}{2} m_\alpha \omega_\alpha^2 [A_\alpha^{(2)}]^2 \sin^2[\omega_\alpha(t - \tau) + \theta_\alpha^{(2)}] \quad (39)$$

$$= \sum_\alpha \frac{1}{2} m_\alpha \omega_\alpha^2 \{ A_\alpha^{(2)} \sin \theta_\alpha^{(2)} \cos[\omega_\alpha(t - \tau)] + A_\alpha^{(2)} \cos \theta_\alpha^{(2)} \sin[\omega_\alpha(t - \tau)] \}^2. \quad (40)$$

Using Eqs. (34) and (37), and then (31) and (32), one can express the amplitudes $A_\alpha^{(2)}$ and phases $\theta_\alpha^{(2)}$ in terms of the initial amplitudes A_α and phases θ_α in Eq. (22) as well as through the velocities u_α introduced in Eq. (36). One obtains, thereby,

$$E_k^{(2)}(t) = \sum_\alpha \frac{1}{2} m_\alpha \omega_\alpha^2 \left\{ -\frac{\lambda_2 u_\alpha}{\omega_\alpha} \cos[\omega_\alpha(t - \tau)] + A_\alpha^{(1)} \cos[\omega_\alpha \tau + \theta_\alpha^{(1)}] \sin[\omega_\alpha(t - \tau)] \right\}^2 \\ = \sum_\alpha \frac{1}{2} m_\alpha \omega_\alpha^2 \left\{ -\frac{\lambda_2 u_\alpha}{\omega_\alpha} \cos[\omega_\alpha(t - \tau)] + \sin[\omega_\alpha(t - \tau)] \left[\frac{\lambda_1 u_\alpha}{\omega_\alpha} \sin \omega_\alpha \tau + A_\alpha \cos \theta_\alpha \cos \omega_\alpha \tau \right] \right\}^2. \quad (41)$$

This expression needs to be averaged over A_α , θ_α , and u_α . Employing Eqs. (24), (25) and (38) one can carry out the necessary averages and obtains

$$\langle E_k^{(2)}(t) \rangle = \left[\frac{(3N-6)k_B T_0}{2} \right] \left\langle \left[\frac{1+\lambda_1^2+2\lambda_2^2}{4} + \frac{1-\lambda_1^2}{4} \cos(2\omega_\alpha \tau) - \frac{1-\lambda_1^2}{8} \cos(2\omega_\alpha t) - \frac{1+\lambda_1^2-2\lambda_2^2}{4} \cos[2\omega_\alpha(t-\tau)] \right. \right. \\ \left. \left. - \frac{1-\lambda_1^2}{8} \cos[2\omega_\alpha(t-2\tau)] + \frac{\lambda_1\lambda_2}{2} \cos\left[2\omega_\alpha\left(t-\frac{\tau}{2}\right)\right] - \frac{\lambda_1\lambda_2}{2} \cos\left[2\omega_\alpha\left(t-\frac{3\tau}{2}\right)\right] \right] \right\rangle_\alpha, \quad (42)$$

where $\langle \dots \rangle_\alpha$ denotes an average over all normal modes as described in Eq. (27). In the above derivation we have employed the property that the average of $u_\alpha A_\alpha$ over A_α and u_α vanishes.

According to Eq. (26), one can replace all occurrences of $\langle \cos[2\omega_\alpha(t-t')] \rangle_\alpha$ by $C_{T,T}(t-t')$. Using Eq. (42), one obtains then for the temperature at $t \geq \tau$

$$T^{(2)}(t) = T_0 \left[\frac{1+\lambda_1^2+2\lambda_2^2}{4} + \frac{1-\lambda_1^2}{4} C_{T,T}(\tau) \right. \\ \left. - \frac{1-\lambda_1^2}{8} C_{T,T}(t) - \frac{1+\lambda_1^2-2\lambda_2^2}{4} C_{T,T}(t-\tau) \right. \\ \left. - \frac{1-\lambda_1^2}{8} C_{T,T}(|t-2\tau|) + \frac{\lambda_1\lambda_2}{2} C_{T,T}\left(t-\frac{\tau}{2}\right) \right. \\ \left. - \frac{\lambda_1\lambda_2}{2} C_{T,T}\left(t-\frac{3\tau}{2}\right) \right]. \quad (43)$$

$C_{T,T}(t)$ decays on a time scale of τ_0 [c.f. Eqs. (28) and (29) and Fig. 5] and, hence, we can note $C_{T,T}(\tau) \approx 0$, $C_{T,T}(t) \approx 0$ and $C_{T,T}(|t-2\tau|) \approx 0$ when $t \gg \tau_0$. This leads to the expression

$$T^{(2)}(t) \approx T_0 \left[\frac{1+\lambda_1^2+2\lambda_2^2}{4} - \frac{1+\lambda_1^2-2\lambda_2^2}{4} C_{T,T}(t-\tau) \right. \\ \left. - \frac{\lambda_1\lambda_2}{2} C_{T,T}\left(t-\frac{3\tau}{2}\right) - \frac{1-\lambda_1^2}{8} C_{T,T}(|t-2\tau|) \right]. \quad (44)$$

new temperature
temperature recovery

3 τ /2-pulse
2 τ -pulse

The terms in this expression can be interpreted in a straightforward way. We first note that the second, third, and fourth term do not contribute, except for $t \approx \tau, 3\tau/2, 2\tau$. The first term, accordingly, describes the average temperature after the second velocity reassignment. The second term describes the recovery of the temperature immediately after the second reassignment, i.e., at $t = \tau$. Since $C_{TT}(0) = 1$ the temperature at $t = \tau$, given by the first two terms in Eq. (44), is $T_2 = \lambda_2^2 T_0$, the expected result. The second term in Eq. (44) describes the relaxation of the temperature from this initial value to the average temperature $\frac{1}{4} T_0 (1 + \lambda_1^2 + 2\lambda_2^2)$. The third term in Eq. (44) describes the $\frac{3}{2}\tau$ -pulse; the prefactor of C_{TT} in this term is the depth $\Delta \bar{T}(3\tau/2)$ of this pulse, i.e.,

$$\Delta \bar{T}\left(\frac{3\tau}{2}\right) = \frac{T_0}{2} \lambda_1 \lambda_2. \quad (45)$$

The fourth term describes the 2τ -pulse; the depth of this pulse is

$$\Delta \bar{T}(2\tau) = \frac{T_0}{8} (1 - \lambda_1^2). \quad (46)$$

A key prediction of Eqs. (45) and (46) is that the echo depths are predicted to be independent of the time interval τ . We will see below that actual simulations reveal a dependence on τ ; anharmonic interactions need to be introduced to repair this deficiency of Eqs. (45) and (46).

If one carries out the derivation above for the set (19) of Maxwellian velocities (at temperature $T_2 = \lambda_2^2 T_0$) which is uncorrelated from the set (16) of Maxwellian velocities (at temperature $T_1 = \lambda_1^2 T_0$) the temperature response $T(t)$ will again be given by Eq. (44), except that the term with $\sim \lambda_1 \lambda_2$ actually vanishes. This implies that a choice of uncorrelated sets (16), (19) abolishes the $\frac{3}{2}\tau$ -echo. On the other hand, one may notice that, in the above derivation, the condition of Maxwellian velocities has not been used. If one applies a velocity set $u_\alpha^{(1)}$ for the first assignment and another velocity set $u_\alpha^{(2)}$ for the second assignment, provided

$$\langle u_\alpha^{(1)} \rangle_u = \langle u_\alpha^{(2)} \rangle_u = 0; \quad \langle u_\alpha^{(1)} u_\alpha^{(2)} \rangle_u \neq 0, \quad (47)$$

even though $u_\alpha^{(1)}$ and $u_\alpha^{(2)}$ may not satisfy the Maxwell distribution (5), Eqs. (30)–(46) still hold and the echo at $3\tau/2$ will remain.

C. Comparison with simulations of the velocity reassignment echo

We want to compare the prediction of expression (44) with simulated echoes. Figure 1(c) demonstrates that Eq. (44) predicts rather well echoes generated by molecular dynamics simulations. The dotted lines presented in Fig. 1(c) correspond to Eq. (44), assuming that the temperature correlation function $C_{T,T}(t)$ vanishes for $t \gg \tau_0$. It is interesting to note that the prediction holds better for the echo at $t = 2\tau$ than for the echo at $t = 3\tau/2$ in terms of the echo shape.

In the case of a CVRE, i.e., for $\lambda_1 = 1$ and $\lambda_2 = 1$, expression (44) reads

$$T^{(2)}(t) \approx T_0 \left[1 - \frac{1}{2} C_{T,T}\left(t - \frac{3\tau}{2}\right) \right]. \quad (48)$$

Figure 2(b) compares a simulated CVRE with the prediction by Eq. (48) for BPTI at $T_0 = 300$ K. The shape of the predicted echo is found in good agreement with that of the simulated echo. However, similarly to the TQE case,²⁹ the depth of the CVRE is not as deep as predicted by the harmonic approximation. We will demonstrate further below

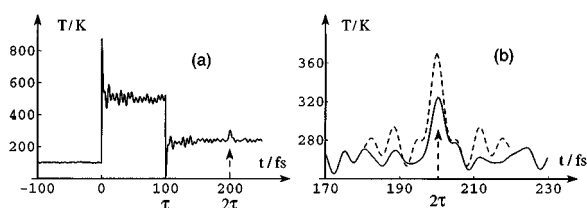


FIG. 6. (a) Temperature response after a velocity reassignment at $t=0$ with temperature $T_1=900$ K and a quench ($T_2=0$ K) at $t=\tau$, starting with an equilibrated protein at $T_0=100$ K ($\tau=100$ fs); (b) enlargement of (a) (solid line) and comparison with the temperature response expressed through (49) (dashed line).

that for τ values significantly larger than 100 fs the depth of the simulated echo decreases rapidly, diverging from the prediction by Eqs. (48) and (44).

We want to finally demonstrate that VREs can yield also “positive” echoes. An example is shown in Fig. 6. In this case BPTI at $T_0=100$ K had been subjected to velocity reassignments with $T_1=900$ K (implying a heat pulse at $t=0$ with $\lambda_1=3$) and $T_2=0$ (implying a quench at $t=\tau$ with $\lambda_2=0$). Expression (44) reads for $\lambda_2=0$

$$T^{(2)}(t) \approx T_0 \left\{ \frac{1+\lambda_1^2}{4} [1 - C_{T,T}(t-\tau)] - \frac{1-\lambda_1^2}{8} C_{T,T}(|t-2\tau|) \right\} \quad (49)$$

and predicts that solely a 2τ -echo arises. We note, in passing, that in the case $\lambda_1=0$ Eq. (49) reproduces the expression for the TQE derived in Ref. 29. For $\lambda_1>1$ expression (49) predicts indeed a positive temperature echo. Such echo, observed also in cool-heat-cool temperature echoes,²⁸ is produced in the simulation presented in Fig. 6. A comparison between the prediction by Eq. (49) and the simulation results in Fig. 6(b) reveals a rather large deviation due to strong anharmonicity at high temperature, which will be discussed below.

VI. PHASE COHERENCE AFTER VELOCITY REASSIGNMENTS

In this section we will demonstrate that the echo at $t=3\tau/2$ in the VRE stems from a coherence of the motion, i.e., from an inhomogeneous phase distribution induced by the velocity reassignments. Essential for the generation of coherence is a correlation between the two sets of velocities (16), (19) employed in the reassignments. To illustrate the relationship between phase coherence or velocity correlation on the one side, and the $\frac{3}{2}\tau$ -echo on the other side, we will focus on the extreme case of a CVRE in which the echo at $t=2\tau$ does not arise. The 2τ -echo, the only echo in case of a TQE, has an origin different from that of the $\frac{3}{2}\tau$ -echo: the temperature quenches, i.e., reassignments of zero velocities, not only set the phases of all modes to 0 and π , but also alter the amplitudes of the modes as demonstrated in Ref. 29; in case of the CVRE, however, the amplitudes of the modes are completely unaffected. We will first demonstrate numerically the existence of phase coherence in case of the CVRE. We

will then provide a simple geometrical argument for the phase coherence and, finally, describe the distribution of the phases after the velocity reassignments.

A. Behavior of an ideal ensemble

A definition of a phase for a system of non-linear oscillators is difficult and, hence, it is essentially impossible to demonstrate phase coherence for a protein described by molecular dynamics simulations. We resort, therefore, to an ensemble of purely harmonic oscillators for which phase and phase coherence are readily defined. For this purpose we consider an ensemble of 10 000 harmonic oscillators at temperature T_0 with frequencies ω_α , $\alpha=1,2,\dots,10\,000$. We assumed a density of states $D(\omega) \propto \sqrt{\omega}$ with a cutoff $0 < \omega < 10$ and selected, accordingly, a set of 10 000 random frequencies ω_α obeying this density; the method employed is the same as in Ref. 29.

To describe the ensemble of oscillators we need to determine a set of amplitudes A_α as well as a set of initial phases θ_α . The amplitudes A_α should obey the Rayleigh distribution (24), i.e., should correspond to an ensemble at temperature T_0 . Rather than employing A_α we introduce mass-weighted amplitudes

$$q_\alpha = \sqrt{m_\alpha/k_B} \omega_\alpha A_\alpha, \quad (50)$$

since this choice will make an additional choice of masses for the ensemble of oscillators unnecessary. The quantities q_α obey the distribution

$$P(q_\alpha) = \frac{q_\alpha}{T_0} \exp\left(-\frac{q_\alpha^2}{2T_0}\right). \quad (51)$$

The phases θ_α are chosen homogeneously distributed in the interval $[0, 2\pi]$.

For the velocity reassignments one needs to select a set of random velocities u_α to be assigned, in case of the CVRE, to each mode at $t=0$ and at $t=\tau$. The u_α 's are distributed according to the Maxwell distribution

$$f(u_\alpha) = \sqrt{\frac{m_\alpha}{2\pi k_B T_0}} \exp\left(-\frac{m_\alpha u_\alpha^2}{2k_B T_0}\right). \quad (52)$$

For this purpose we employ again mass-weighted quantities, namely,

$$\gamma_\alpha = \sqrt{m_\alpha/k_B} u_\alpha, \quad (53)$$

which obey the distribution

$$f(\gamma_\alpha) = \frac{1}{\sqrt{2\pi T_0}} \exp\left(-\frac{\gamma_\alpha^2}{2T_0}\right). \quad (54)$$

We will show now that the phases of the ensemble of oscillators after the first and the second velocity reassignment, i.e., the phases $\theta_\alpha^{(1)}$ and $\theta_\alpha^{(2)}$ as defined in Eqs. (30), (33), can be expressed in terms of the selected quantities ω_α , q_α , γ_α and θ_α , $\alpha=1,2,\dots,10\,000$. According to Eqs. (31) and (32), the phases after the first velocity reassignment, $\theta_\alpha^{(1)}$, can be determined through

$$\cot \theta_\alpha^{(1)} = -\frac{A_\alpha \omega_\alpha \cos \theta_\alpha}{u_\alpha} = -\frac{q_\alpha \cos \theta_\alpha}{\gamma_\alpha}, \quad (55)$$

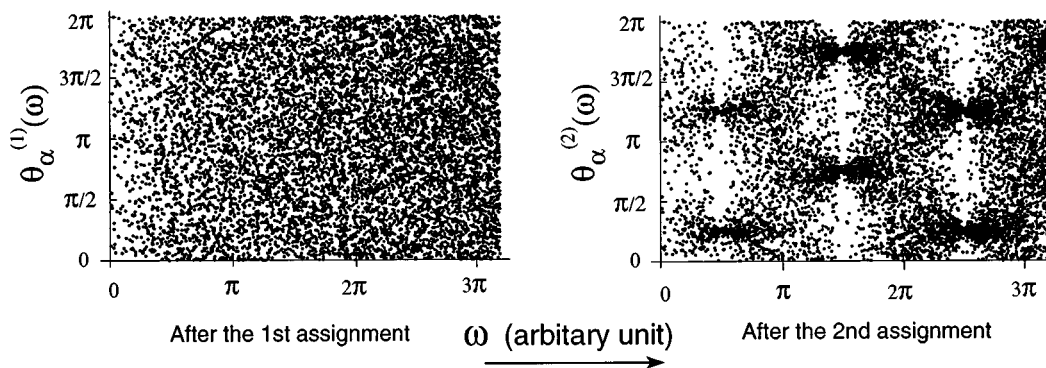


FIG. 7. Distribution of phases $\theta_\alpha^{(1)}$ and $\theta_\alpha^{(2)}$, $\alpha=1,2,\dots,10\,000$, after constant temperature velocity reassignments for a time interval $\tau=1$ ($T_0=T_1=T_2=300$ K); each point in the figure represents a specific $(\omega_\alpha, \theta_\alpha)$ -tuple determined according to Eqs. (55) and (56).

where the sign of $\cos \theta_\alpha^{(1)}$ is the same as that of $\cos \theta_\alpha$. The phases after the second velocity reassignment, $\theta_\alpha^{(2)}$, can be calculated from Eqs. (34), (37), (31), (32). One obtains

$$\begin{aligned} \cot \theta_\alpha^{(2)} &= -\frac{A_\alpha^{(1)} \omega_\alpha \cos(\omega_\alpha \tau + \theta_\alpha^{(2)})}{u_\alpha} \\ &= -\frac{A_\alpha \omega_\alpha \cos(\omega_\alpha \tau) \cos \theta_\alpha + \sin(\omega_\alpha \tau)}{u_\alpha} \\ &= -\xi_\alpha \cos(\omega_\alpha \tau) + \sin(\omega_\alpha \tau), \end{aligned} \quad (56)$$

where

$$\xi_\alpha = q_\alpha \cos \theta_\alpha / \gamma_\alpha. \quad (57)$$

The sign of $\cos \theta_\alpha^{(2)}$, according to Eq. (34), is identical to that of $\cos(\omega_\alpha \tau + \theta_\alpha^{(1)})$. We employed the program package MATHEMATICA⁴⁰ to evaluate $\theta_\alpha^{(1)}$ and $\theta_\alpha^{(2)}$ for all 10 000 modes.

Figure 7 presents the resulting phases. The figure demonstrates that the phases $\theta_\alpha^{(1)}$ are homogeneously distributed in the interval $[0, 2\pi]$, but that the phases $\theta_\alpha^{(2)}$ exhibit a distinctly inhomogeneous distribution. In fact, modes with frequencies near $\omega_\alpha = (n+1/2)\pi/\tau$ assume phases $\theta_\alpha^{(2)}$ with values concentrated around $\pi/4$, $3\pi/4$, $5\pi/4$ and $7\pi/4$. This behavior is consistent with expression (56), since $\cot \theta_\alpha^{(2)} = 1$ for $\omega_\alpha = (n+1/2)\pi/\tau$. As a result, modes with frequencies $\omega_\alpha = (n+1/2)\pi/\tau$ will assume vanishing velocities at time $t=3\pi/2$ inducing, thereby, the $\frac{3}{2}\tau$ -echo in the kinetic energy or temperature.

B. Geometric construction of phases

To shed further light on the phase coherence illustrated in Fig. 7 we follow the phases of the system through the coordinate-velocity phase trajectories of the individual oscillators. Choosing mass-weighted coordinates y_α and velocities \dot{y}_α , i.e., $y_\alpha = \sqrt{m_\alpha/k_B} \omega_\alpha x_\alpha$ and $\dot{y}_\alpha = \sqrt{m_\alpha/k_B} \dot{x}_\alpha$, the trajectories $(y_\alpha(t), \dot{y}_\alpha(t))$ move counter-clockwise on circles with frequency $\omega = \pi/2\tau$. The motion and its change upon velocity replacements is schematically presented in Fig. 8.

Before the first velocity reassignment, the normal mode moves counterclockwise along the outer circle in Fig. 8. Let $A = (\tilde{y}_\alpha, \tilde{\dot{y}}_\alpha)$ denote the phase space point where the first

velocity reassignment occurs. Assume the mass-weighted velocity, randomly assigned to the mode, is u_0 . After the velocity reassignment, the trajectory resumes its counterclockwise circular motion starting at $B = (\tilde{y}'_\alpha, u_0)$, i.e., on the middle circle in Fig. 8. At $t=\tau$ the mode will reach point $C = (\tilde{y}'_\alpha, \tilde{\dot{y}}'_\alpha)$. After the second velocity reassignment the normal mode resumes its counterclockwise circular motion on the inner circle in Fig. 8, starting at $D = (\tilde{y}'_\alpha, u_0)$. Since $OC=OB$, and $\angle BOL = \angle COQ = \angle MCO$, $\triangle OLB \cong \triangle CMO$, we can conclude $OM=BL=DM$, i.e., $\angle DOM = \pi/4$. This means that, at time $t=3\pi/2$, the normal mode, in case $\omega\tau = \pi/2$, will reach point E , which corresponds to vanishing velocity. Accordingly, a mode with frequency $\omega = \pi/2\tau$, together with modes with close frequencies, contributes nearly vanishing kinetic energy at $t=3\pi/2$ and, accordingly, participates in the generation of the echo.

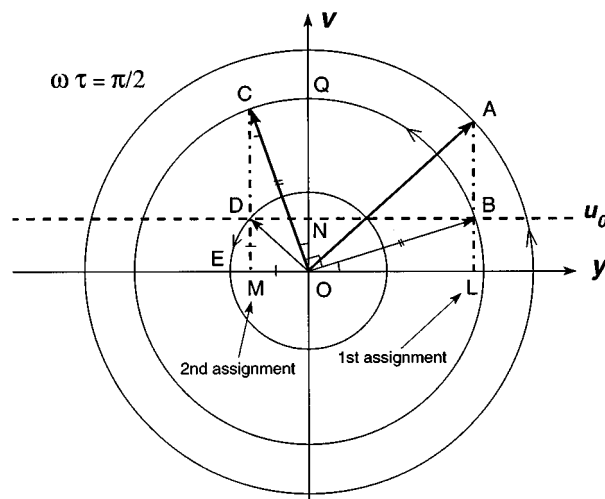


FIG. 8. Coordinate-velocity diagram of a mode with frequency $\omega = \pi/2\tau$ in case of a CVRE; before the first velocity reassignment, the normal mode moves counter-clockwise along the outer circle; the first velocity assignment corresponds to the transition $A \rightarrow B$; between the first velocity reassignment and the second one, the mode moves counter-clockwise along the middle circle, from B to C ; the second assignment corresponds to the transition $C \rightarrow D$; after the second velocity assignment, the mode moves counter-clockwise along the inner circle, starting from D .

C. Phase distribution after the second reassignment

We want to characterize now the distribution of the phases $\theta_\alpha^{(2)}$ for arbitrary ω_α through the median value and the variance of the distribution. Analytical expressions for the variance of $\theta_\alpha^{(2)}$ cannot be obtained, but one can determine the variance of $\cot \theta_\alpha^{(2)}$ instead. We note for this purpose that ξ_α in Eq. (56) is independent of ω_α . Accordingly, the variance of $\cot \theta_\alpha^{(2)}$ is

$$\sigma(\cot \theta_\alpha^{(2)}) = \cos^2(\omega_\alpha \tau) \sigma_0(\xi_\alpha), \quad (58)$$

where $\sigma_0(\xi_\alpha)$ is a constant and, choosing suitable units, may be set to unity.

In order to determine the median of $\theta_\alpha^{(2)}$, we consider the average of $\cot \theta_\alpha^{(2)}$ in Eq. (56)

$$\langle \cot \theta_\alpha^{(2)} \rangle = \sin(\omega_\alpha \tau). \quad (59)$$

Defining

$$\cot \bar{\theta}_\alpha = \langle \cot \theta_\alpha^{(2)} \rangle, \quad (60)$$

one obtains

$$\bar{\theta}_\alpha = \arccot[\sin(\omega_\alpha \tau)] + n\pi, \quad (61)$$

where n is 0 and ± 1 ; the sign of ± 1 is determined to ensure $\bar{\theta}_\alpha$ to lie in the interval $[0, 2\pi]$. $\bar{\theta}_\alpha$ is the median of $\theta_\alpha^{(2)}$. In fact, since ξ_α is distributed symmetrically around 0 [cf. Eq. (57)] and since the $\cot(x)$ function is one-to-one homologous to x in the range of $[0, \pi]$ or of $[\pi, 2\pi]$, the number of modes for $\theta_\alpha^{(2)} > \bar{\theta}_\alpha$ should be the same as that for $\theta_\alpha^{(2)} < \bar{\theta}_\alpha$ when $0 \leq \theta_\alpha^{(2)} < \pi$ or $\pi \leq \theta_\alpha^{(2)} < 2\pi$. This means that $\bar{\theta}_\alpha$ separates the distribution $p_\alpha(\theta_\alpha^{(2)})$ such that

$$\int_{k\pi}^{\bar{\theta}_\alpha} d\theta_\alpha p_\alpha(\theta_\alpha^{(2)}) = \int_{\bar{\theta}_\alpha}^{(k+1)\pi} d\theta_\alpha p_\alpha(\theta_\alpha^{(2)}), \quad k=0,1 \quad (62)$$

which identifies $\bar{\theta}_\alpha$ as the median (central value) of $\theta_\alpha^{(2)}$.

Figure 9 presents $\bar{\theta}_\alpha$ and $\sigma(\cot \theta_\alpha^{(2)})$ as a function of ω_α . For modes with frequencies $\omega_\alpha = (n+1/2)\pi/\tau$, $\bar{\theta}_\alpha$ is seen to assume values $\pi/2 \pm \pi/4$ for $0 \leq \theta_\alpha^{(2)} < \pi$, and values $3\pi/2 \pm \pi/4$ for $\pi \leq \theta_\alpha^{(2)} < 2\pi$. Figure 9 also shows that the variance of $\cot \theta_\alpha$ for modes with frequencies close to $\omega_\alpha = (n+1/2)\pi/\tau$ is very small. One can conclude that modes near $\omega_\alpha = (n+1/2)\pi/\tau$ lock their phases and, thereby contribute to the VRE. Modes with frequencies which differ significantly from $\omega_\alpha = (n+1/2)\pi/\tau$ have large variance, indicative of a lack of coherence; such modes basically do not contribute significantly to the VRE.

VII. PHASE DIFFUSION MODEL

In the framework of the harmonic approximation one can describe accurately the position and the width of the two echoes after the velocity reassignments and account approximately for the shape of the echoes, including their side bands (cf. Fig. 7 in Ref. 29). However, in the harmonic approximation one predicts that the depth of the echoes is independent of the time interval τ between velocity replacements; simulations presented in Ref. 29 and in this article reveal that the echo depth in proteins shows a strong dependence on the

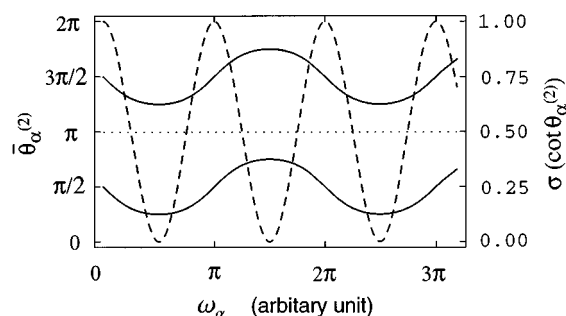


FIG. 9. $\bar{\theta}_\alpha^{(2)}$, the median of $\theta_\alpha^{(2)}$, in the range $[0, \pi]$ and $[\pi, 2\pi]$ respectively (solid lines) and the variance of $\cot \theta_\alpha^{(2)}$, as given by Eq. (58) (dashed line). The unit for $\sigma(\cot \theta_\alpha^{(2)})$ is rescaled such that $\sigma_0(\xi_\alpha) = 1$ ($\tau = 1$).

time interval τ . The aim of the present section is to explain the mechanism underlying this τ -dependence.

Most revealing for this mechanism is a consideration of the CVRE (cf. Fig. 10): in this case, the velocity reassignments leave the distribution of the normal mode amplitudes unaltered, only the phases being affected; hence, phase relaxation due to anharmonic interactions must be a main cause of the observed τ -dependence. In the following we are guided by the discussions regarding the TQE presented in Refs. 27,41 and by the successful description of the depth of TQEs in Ref. 29. We will devise a stochastic model for the relaxation of the phases θ_α of the protein modes.

The model applied to describe the phase relaxation of protein modes due to anharmonic interactions had been introduced in Ref. 29. In the harmonic approximation the motion of the α th normal mode is described by the expression $A_\alpha \sin(\omega_\alpha t + \theta_\alpha)$. The interaction of the mode with the other normal modes, due to the anharmonic interactions, involves a large number of independent contributions such that one may consider the interaction as stochastic. Both the amplitude A_α and the phase θ_α will be affected, but at present we focus solely on the relaxation of the phase. We account for this relaxation through an additive random phase δ_α replacing $\theta_\alpha \rightarrow \theta_\alpha + \delta_\alpha$. Assuming, for the moment, $\theta_\alpha = 0$, the motion of normal modes subject to anharmonic interactions is then described by $A_\alpha \sin(\omega_\alpha t + \delta_\alpha)$.

We assume that the random phase δ_α is described by a Wiener process. Such process also describes Brownian motion and, accordingly, we refer to the present model as the phase diffusion model. This model is consistent with the picture in which the time derivative of δ_α obeys $\dot{\delta}_\alpha = \eta(t)$ where $\eta(t)$ presents white noise. The Wiener process is characterized through⁴²

$$\langle \delta_\alpha(t) \rangle = 0 \quad (63)$$

$$\langle \delta_\alpha(t_1) \delta_\alpha(t) \rangle = 2\gamma_\alpha T \min(t_1, t).$$

We have included in the above formula the assumption that the noise amplitude increases linearly with temperature such

that γ_α represents a temperature-independent constant. The probability to observe a phase δ_α at time t , when the phase is zero at $t=0$, is

$$P(\delta_\alpha, t) = \frac{1}{\sqrt{4\pi\gamma_\alpha T t}} \exp\left(-\frac{\delta_\alpha^2}{4\gamma_\alpha T t}\right). \quad (64)$$

To account for the effect of phase randomization one introduces the quantities $\delta_{\alpha,1}(t)$ and $\delta_{\alpha,2}(t)$ which describe the additional random phases developing after the first velocity reassignment and after the second velocity reassignment, respectively. Accordingly, one replaces Eqs. (30), (33) by

$$x_\alpha^{(1)}(t) = A_\alpha^{(1)} \cos[\omega_\alpha t + \theta_\alpha^{(1)} + \delta_{\alpha,1}(t)]; \quad (65)$$

$$x_\alpha^{(2)}(t) = A_\alpha^{(2)} \cos[\omega_\alpha(t-\tau) + \theta_\alpha^{(2)} + \delta_{\alpha,2}(t-\tau)] \quad (66)$$

and employs these expressions to evaluate the kinetic energy. The kinetic energy after the second velocity reassignment is then [cf. Eq. (39)]

$$E_k^{(2)}(t) = \sum_\alpha \frac{1}{2} m_\alpha \omega_\alpha^2 (A_\alpha^{(2)})^2 \sin^2[\omega_\alpha(t-\tau) + \theta_\alpha^{(2)} + \delta_{\alpha,2}(t-\tau)]. \quad (67)$$

Using Eqs. (34) and (37) and taking into account the random phase developing after the first velocity reassignment until $t=\tau$, i.e., $\delta_{\alpha,1}(\tau)$, one obtains

$$E_k^{(2)}(t) = \sum_\alpha \frac{1}{2} m_\alpha \omega_\alpha^2 \left[-\frac{\lambda_2 u_\alpha}{\omega_\alpha} \cos[\omega_\alpha(t-\tau) + \delta_{\alpha,2}(t-\tau)] + A_\alpha^{(1)} \cos[\omega_\alpha \tau + \theta_\alpha^{(1)} + \delta_{\alpha,1}(\tau)] \sin[\omega_\alpha(t-\tau) + \delta_{\alpha,2}(t-\tau)] \right]^2. \quad (68)$$

Applying the conditions (31) and (32), this can be written

$$E_k^{(2)}(t) = \sum_\alpha \frac{1}{2} m_\alpha \omega_\alpha^2 \left\{ -\frac{\lambda_2 u_\alpha}{\omega_\alpha} \cos[\omega_\alpha(t-\tau) + \delta_{\alpha,2}(t-\tau)] + \sin[\omega_\alpha(t-\tau) + \delta_{\alpha,2}(t-\tau)] \times \left(\frac{\lambda_1 u_\alpha}{\omega_\alpha} \sin[\omega_\alpha \tau + \delta_{\alpha,1}(\tau)] + A_\alpha \cos\theta_\alpha \cos[\omega_\alpha \tau + \delta_{\alpha,1}(\tau)] \right) \right\}^2. \quad (69)$$

The average over A_α , θ_α , and u_α , employing Eqs. (24), (25) and (38), results in an expression similar to Eq. (42)

$$\begin{aligned} \langle E_k^{(2)}(t) \rangle = & \frac{(3N-6)k_B T_0}{2} \left\langle \frac{1+\lambda_1^2+2\lambda_2^2}{4} + \frac{1-\lambda_1^2}{4} \cos[2\omega_\alpha \tau + 2\delta_{\alpha,1}(\tau)] - \frac{1-\lambda_1^2}{8} \cos[2\omega_\alpha t + 2\delta_{\alpha,1}(\tau) + 2\delta_{\alpha,2}(t-\tau)] \right. \\ & - \frac{1+\lambda_1^2-2\lambda_2^2}{4} \cos[2\omega_\alpha(t-\tau) + 2\delta_{\alpha,2}(t-\tau)] - \frac{1-\lambda_1^2}{8} \cos[2\omega_\alpha(t-2\tau) - 2\delta_{\alpha,1}(\tau) + 2\delta_{\alpha,2}(t-\tau)] \\ & \left. + \frac{\lambda_1\lambda_2}{2} \cos\left[2\omega_\alpha\left(t-\frac{\tau}{2}\right) + \delta_{\alpha,1}(\tau) + 2\delta_{\alpha,2}(t-\tau)\right] - \frac{\lambda_1\lambda_2}{2} \cos\left[2\omega_\alpha\left(t-\frac{3\tau}{2}\right) - \delta_{\alpha,1}(\tau) + 2\delta_{\alpha,2}(t-\tau)\right] \right\rangle_\alpha. \quad (70) \end{aligned}$$

This expression contains, however, the random phases $\delta_{\alpha,1}(\tau)$ and $\delta_{\alpha,2}(t-\tau)$. We have replaced here the sum over all modes α by the average $\langle \dots \rangle_\alpha$.

In order to determine the kinetic energy observed for an ensemble of oscillators one needs to average expression (70) over the phases $\delta_{\alpha,1}(\tau)$ and $\delta_{\alpha,2}(t-\tau)$ using the appropriate probabilities. Noting that the average temperature after the first velocity reassignment, is $(1+\lambda_1^2)T_0/2$, the distribution for $\delta_{\alpha,1}(t)$ is

$$P(\delta_{\alpha,1}(t), t) = \frac{1}{\sqrt{2(1+\lambda_1^2)\pi\gamma_\alpha T_0 t}} \times \exp\left[-\frac{\delta_{\alpha,1}^2(t)}{2(1+\lambda_1^2)\gamma_\alpha T_0 t}\right]. \quad (71)$$

Since the average temperature after the second velocity reassignment is $(1+\lambda_1^2+2\lambda_2^2)T_0/4$, the distribution for $\delta_{\alpha,2}(t)$ is

$$P(\delta_{\alpha,2}(t), t) = \frac{1}{\sqrt{(1+\lambda_1^2+2\lambda_2^2)\pi\gamma_\alpha T_0 t}} \times \exp\left[-\frac{\delta_{\alpha,2}^2(t)}{(1+\lambda_1^2+2\lambda_2^2)\gamma_\alpha T_0 t}\right]. \quad (72)$$

The term which contributes in Eq. (70) to the echo at $t=3\tau/2$ is

$$I(t) = -\frac{(3N-6)k_B T \lambda_1 \lambda_2}{2} \left\langle \left\langle \cos \left[2\omega_\alpha \left(t - \frac{3\tau}{2} \right) - \delta_{\alpha,1}(\tau) + 2\delta_{\alpha,2}(t-\tau) \right] \right\rangle \right\rangle_{\zeta_\alpha} \quad (73)$$

The depth $\Delta T(3\tau/2)$ of the temperature echo is given by $-[2/(3N-6)k_B]I(3\tau/2)$. The phases $\delta_{\alpha,1}(\tau)$ and $\delta_{\alpha,2}(t-\tau)$ occur in Eq. (73) in the combination

$$\zeta_\alpha = -\delta_{\alpha,1}(\tau) + 2\delta_{\alpha,2}(\tau/2). \quad (74)$$

Since $\delta_{\alpha,1}(\tau)$ and $\delta_{\alpha,2}(\tau/2)$ are independent Gaussian random variables, the distribution of ζ_α is then again Gaussian, namely,

$$f(\zeta_\alpha) = \frac{1}{\sqrt{4(1+\lambda_1^2+\lambda_2^2)\pi\gamma_\alpha T_0 \tau}} \times \exp\left[-\frac{\zeta_\alpha^2}{4(1+\lambda_1^2+\lambda_2^2)\gamma_\alpha T_0 \tau}\right]. \quad (75)$$

Accordingly, one can express the average over $\delta_{\alpha,1}(\tau)$ and $\delta_{\alpha,2}(t-\tau)$ at $t=3\tau/2$ by an average over ζ_α , using the distribution (75). The echo depth can then be written

$$\Delta T(3\tau/2) = \frac{\lambda_1 \lambda_2 T_0}{2} \left\langle \int_{-\infty}^{\infty} d\zeta_\alpha \cos(\zeta_\alpha) \times \frac{1}{\sqrt{4(1+\lambda_1^2+\lambda_2^2)\pi\gamma_\alpha T_0 \tau}} \times \exp\left(-\frac{\zeta_\alpha^2}{4(1+\lambda_1^2+\lambda_2^2)\gamma_\alpha T_0 \tau}\right) \right\rangle_{\alpha}. \quad (76)$$

The integral can be evaluated and one obtains

$$\Delta T(3\tau/2) = \frac{\lambda_1 \lambda_2 T_0}{2} \langle \exp[-(1+\lambda_1^2+\lambda_2^2)\gamma_\alpha T_0 \tau] \rangle_{\alpha}. \quad (77)$$

If one assumes γ_α is the same constant γ_0 for all modes, this yields finally

$$\Delta T(3\tau/2) = \frac{\lambda_1 \lambda_2 T_0}{2} \exp[-(1+\lambda_1^2+\lambda_2^2)\gamma_0 T_0 \tau]. \quad (78)$$

Similarly, one can derive for the echo at $t=2\tau$

$$\Delta T(2\tau) = \frac{(1-\lambda_1^2)T_0}{8} \exp[-(3+3\lambda_1^2+2\lambda_2^2)\gamma_0 T_0 \tau]. \quad (79)$$

Figure 10 shows that the depths of the simulated echoes, in case of CVREs, i.e., for $\lambda_1=\lambda_2=1$, fit a mono-exponential decay. $\Delta T(3\tau/2) \propto e^{-t/\tau_c}$. From (78) and for $\lambda_1=\lambda_2=1$ one expects the relationship

$$\frac{1}{\tau_c} = 3\gamma_0 T_0 \quad (80)$$

to hold, i.e., $1/\tau_c$ should be linearly dependent on the temperature T_0 if γ_0 is indeed to be temperature-independent.

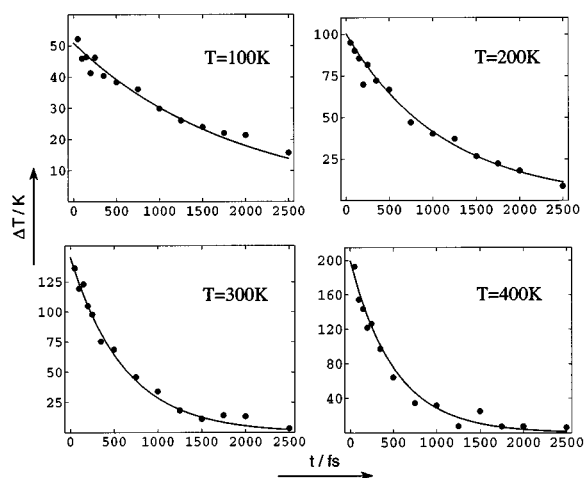


FIG. 10. Depth of echo versus τ in case of CVREs at four different temperatures; the dots are from simulations; the solid lines are least-square fits to the simulation data and yield the relaxation times $\tau_c(T_0)$ employed in Fig. 11.

The simulation results, presented in Fig. 11, verify the expected behavior. This result justifies *a posteriori* the temperature dependence in Eq. (63).

According to Eqs. (78) and (79), the decay times, in case of TQE and CVRE for the same T_0 , should be identical, i.e., should measure $1/(3\gamma_0 T_0)$. However, simulations at $T_0=300$ K yield a decay time of 614.7 fs in case of a CVRE, and a decay time of 833.7 fs²⁹ in case of a TQE. To explain this difference we note that in Eq. (35), condition (20) is applied, i.e., normal modes were assigned the same velocities at $t=0$ and at $t=\tau$, except for a mode-independent factor λ . However, as discussed in Section V, Eq. (20) holds only approximately. If one employs, in the derivation of the echo depth, the velocity set (17) rather than (19), i.e., applies condition (21) instead of (20), expression (79) still holds since the term corresponding to the 2τ -echo in Eq. (70) does not involve any cross term of $u_\alpha^{(1)}$ and $\tilde{u}_\alpha^{(2)}$. However, the expression for $\Delta T(3\tau/2)$, given by Eq. (78), stems from a term containing a factor $\langle u_\alpha^{(1)} \tilde{u}_\alpha^{(2)} \rangle_u$ in Eqs. (70). Accordingly, $\Delta T(3\tau/2)$ for condition (21) becomes

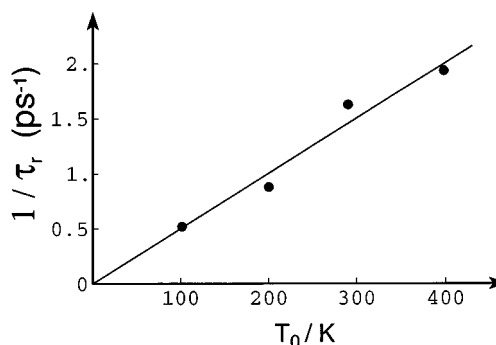


FIG. 11. $1/\tau_c$ versus T_0 in case of CVREs. The data points are from results presented in Fig. 10; the solid line is a least-square fit to the simulation data in a linear form, i.e., $1/\tau_c = cT_0$, where c is determined to be 5.02 (ns K)⁻¹.

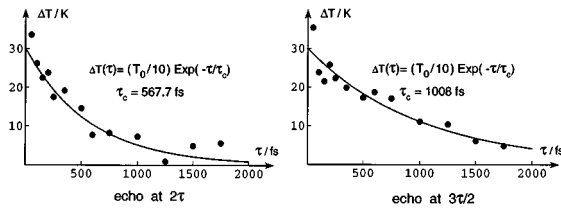


FIG. 12. Depth of VREs at $t=2\tau$ and at $t=3\tau/2$ for the case of $T_1=T_2=60$ K and $T_0=300$ K; the data points are from simulations of BPTI; the solid lines represent least-square fits to the simulation data according to Eqs. (78) and (79).

$$\Delta T(3\tau/2) = \frac{\lambda_1 \lambda_2 T_0}{2} g(\tau, T) \times \exp[-(1 + \lambda_1^2 + \lambda_2^2) \gamma_0 T_0 \tau]. \quad (81)$$

We have assumed here that $g_\alpha(\tau, T)$ is identical for all the modes, i.e., $g_\alpha(\tau, T) = g(\tau, T)$. Since $g(\tau, T)$ is expected to decrease with increasing τ , the decay time of the $\frac{3}{2}\tau$ -echo, in actual simulations, should be smaller than predicted by Eq. (78).

The discrepancy discussed above is also revealed in general VREs. It is expected from Eqs. (78) and (79) that the decay time of the echo at $t=3\tau/2$, i.e., $\tau_c(3\tau/2)$, and the decay time of the echo at $t=2\tau$, i.e., $\tau_c(2\tau)$, should satisfy

$$(1 + \lambda_1^2 + \lambda_2^2) \tau_c(3\tau/2) = (3 + 3\lambda_1^2 + 2\lambda_2^2) \tau_c(2\tau) = \frac{1}{\gamma_0 T_0}. \quad (82)$$

The simulations presented in Fig. 12 started from an equilibrated structure at $T_0=300$ K, and then reassigned twice the same Maxwellian velocities at $T_1=T_2=60$ K, i.e., the simulations realize a VRE with $\lambda_1^2=\lambda_2^2=1/5$. As shown in Fig. 12, the simulations reproduce very well the exponential decay of echo depth as well as the prefactor $T_0/10$ predicted by Eqs. (78), (79). However, a comparison of the decay times of the $\frac{3}{2}\tau$ -echo and the 2τ echo yields

$$\frac{(1 + \lambda_1^2 + \lambda_2^2) \tau_c(3\tau/2)}{(3 + 3\lambda_1^2 + 2\lambda_2^2) \tau_c(2\tau)} = \frac{1.4 \times 1008}{4 \times 567.7} = 0.62 \quad (83)$$

which differs from the value 1 predicted by Eq. (82). This deficiency arises from $g(\tau, T)$ [cf. Eq. (21)] being significantly smaller than unity in the actual simulations.

VIII. LANGEVIN DYNAMICS DESCRIPTION

One can also approach the τ -dependence of the echo depth through a model of an ensemble of oscillators governed by the Langevin equation^{43,44}

$$\ddot{x}_\alpha + b_\alpha \dot{x}_\alpha + \omega_\alpha^2 x_\alpha = \eta_\alpha(t). \quad (84)$$

In this model anharmonic interactions are accounted for through friction $b_\alpha \dot{x}_\alpha$ and fluctuating forces $\eta_\alpha(t)$ which satisfy the fluctuation-dissipation theorem

$$\langle \eta_\alpha(0) \eta_\alpha(t) \rangle = 2k_B T_0 b_\alpha \delta(t) / m_\alpha. \quad (85)$$

We assume that all modes are under-damped, i.e., $\omega_\alpha > \frac{1}{2}b_\alpha$, an assumption which we will justify below, and define the real quantity

$$\Omega_\alpha = \sqrt{\omega_\alpha^2 - \frac{1}{4}b_\alpha^2}. \quad (86)$$

For the temperature echo one needs to determine the average kinetic energy of the ensemble of Langevin oscillators (84). For this purpose the average quantities $\langle x \rangle$, $\langle x^2 \rangle$, $\langle v \rangle$ and $\langle v^2 \rangle$ for a given initial position $x_\alpha(0)$ and velocity $v_\alpha(0)$ of Langevin oscillators will be required. These quantities are given by the expressions

$$\langle x_\alpha(t) \rangle = x_\alpha(0) e^{-b_\alpha t/2} \left[\cos(\Omega_\alpha t) + \frac{b_\alpha}{2\Omega_\alpha} \sin(\Omega_\alpha t) \right] + \frac{v_\alpha(0)}{\Omega_\alpha} e^{-b_\alpha t/2} \sin(\Omega_\alpha t), \quad (87)$$

$$\langle x_\alpha^2(t) \rangle = \langle x_\alpha(t) \rangle^2 + \frac{k_B T_0}{m_\alpha \omega_\alpha^2} \left\{ 1 - e^{-b_\alpha t} \left[\frac{b_\alpha^2}{2\Omega_\alpha^2} \sin^2(\Omega_\alpha t) + \frac{b_\alpha}{2\Omega_\alpha} \sin(2\Omega_\alpha t) + 1 \right] \right\}, \quad (88)$$

$$\langle v_\alpha(t) \rangle = -\frac{x_\alpha(0) \omega_\alpha^2}{\Omega_\alpha} e^{-b_\alpha t/2} \sin(\Omega_\alpha t) + v_\alpha(0) e^{-b_\alpha t/2} \left[\cos(\Omega_\alpha t) - \frac{b_\alpha}{2\Omega_\alpha} \sin(\Omega_\alpha t) \right], \quad (89)$$

$$\langle v_\alpha^2(t) \rangle = \langle v_\alpha(t) \rangle^2 + \frac{k_B T_0}{m_\alpha} \left\{ 1 - e^{-b_\alpha t} \left[\frac{b_\alpha^2}{2\Omega_\alpha^2} \sin^2(\Omega_\alpha t) - \frac{b_\alpha}{2\Omega_\alpha} \sin(2\Omega_\alpha t) + 1 \right] \right\}, \quad (90)$$

which follow from Eq. (214) in Ref. 45.

We will consider in the following the special case of a constant temperature velocity reassignment echo (CVRE) characterized through assigning twice the same velocities u_α to all modes. In order to determine the kinetic energy we consider again, in sequence, three periods: before the first velocity reassignment ($t < 0$), after the first and before the second velocity reassignment ($0 \leq t < \tau$), and after the second velocity reassignment ($t \geq \tau$).

1. Before the first velocity reassignment

In the present situation, this period does not need to be described in detail. All that is required is information on the positions at the end of this period, namely, $x_\alpha^{(0)}(0)$. In fact, we solely need the average values

$$\langle x_\alpha^{(0)}(0) \rangle_{(0)} = 0, \quad \langle [x_\alpha^{(0)}(0)]^2 \rangle_{(0)} = \frac{k_B T_0}{m_\alpha \omega_\alpha^2}, \quad (91)$$

as becomes evident below. Here $\langle \dots \rangle_{(0)}$ denotes the average for the system before the first reassignment. Since the velocities are reassigned at $t=0$, no information on the velocities $v_\alpha(0)$ is required.

2. After the first and before the second velocity reassignment

From this period of the dynamics again only the positions at time $t = \tau$, i.e., $x_\alpha^{(1)}(t)$, are required since the velocities will be reassigned. In fact, one needs solely the averages of $x_\alpha^{(1)}(t)$ and of $[x_\alpha^{(1)}(t)]^2$. Using Eqs. (87) and (88) one obtains for specific initial positions $x_\alpha^{(1)}(0) = x_\alpha^{(0)}(0)$ and assigned velocities $v_\alpha^{(1)}(0) = u_\alpha$

$$\langle x_\alpha^{(1)}(\tau) \rangle_{(1)} = x_\alpha^{(0)}(0) e^{-b_\alpha \tau/2} \left[\cos(\Omega_\alpha \tau) + \frac{b_\alpha}{2\Omega_\alpha} \sin(\Omega_\alpha \tau) \right] + \frac{u_\alpha}{\Omega_\alpha} e^{-b_\alpha \tau/2} \sin(\Omega_\alpha \tau), \quad (92)$$

$$\langle [x_\alpha^{(1)}(\tau)]^2 \rangle_{(1)} = \langle x_\alpha^{(1)}(\tau) \rangle_{(1)}^2 + \frac{k_B T_0}{m_\alpha \omega_\alpha^2} \left\{ 1 - e^{-b_\alpha \tau} \left[\frac{b_\alpha^2}{2\Omega_\alpha^2} \times \sin^2(\Omega_\alpha \tau) + \frac{b_\alpha}{2\Omega_\alpha} \sin(2\Omega_\alpha \tau) + 1 \right] \right\}. \quad (93)$$

In using these quantities below one needs to carry out the averages over all positions $x_\alpha^{(0)}(0)$, denoted by $\langle \dots \rangle_{(0)}$, and over all velocities u_α , denoted by $\langle \dots \rangle_u$.

3. After the second velocity reassignment

From this period one seeks solely information on the velocities in order to determine the average kinetic energy. For specific initial positions $x_\alpha^{(2)}(\tau) = x_\alpha^{(1)}(\tau)$ and assigned velocities $v_\alpha^{(2)}(\tau) = u_\alpha$ follows, using Eqs. (89) and (90),

$$\langle v_\alpha^{(2)}(t) \rangle_{(2)} = - \frac{x_\alpha^{(1)}(\tau) \omega_\alpha^2}{\Omega_\alpha} e^{-b_\alpha(t-\tau)/2} \sin \Omega_\alpha(t-\tau) + u_\alpha e^{-b_\alpha(t-\tau)/2} \left[\cos \Omega_\alpha(t-\tau) - \frac{b_\alpha}{2\Omega_\alpha} \sin \Omega_\alpha(t-\tau) \right], \quad (94)$$

$$\langle [v_\alpha^{(2)}(t)]^2 \rangle_{(2)} = \langle v_\alpha^{(2)}(t) \rangle_{(2)}^2 + \frac{k_B T_0}{m_\alpha} \left\{ 1 - e^{-b_\alpha(t-\tau)} \times \left[\frac{b_\alpha^2}{2\Omega_\alpha^2} \sin^2 \Omega_\alpha(t-\tau) - \frac{b_\alpha}{2\Omega_\alpha} \sin 2\Omega_\alpha(t-\tau) + 1 \right] \right\}. \quad (95)$$

In using these quantities below one needs to carry out the averages over all positions $x_\alpha^{(1)}(\tau)$, denoted by $\langle \dots \rangle_{(1)}$, and over all velocities u_α , denoted by $\langle \dots \rangle_u$. Note that the velocities u_α must be averaged simultaneously for (94) and (95) and (92) and (93) since the same velocities are assigned at $t=0$ and at $t=\tau$.

4. Evaluation of the temperature echo

The average kinetic energy and, hence, the depth of the temperature echo, can be determined from Eqs. (94) and (95) after the following additional averages are being taken:

- (1) average $\langle \dots \rangle_{(1)}$ over all initial positions $x_\alpha^{(1)}(\tau)$, employing Eqs. (92) and (93);
- (2) average $\langle \dots \rangle_{(0)}$ over all initial positions $x_\alpha^{(1)}(0)$, employing Eq. (91);
- (3) average $\langle \dots \rangle_u$ over all reassigned velocities u_α using $\langle u_\alpha \rangle = 0$ and Eq. (38);
- (4) average $\langle \dots \rangle_\alpha$ over all modes α .

One obtains in this way for the echo depth

$$\Delta T(3\tau/2) = T_0 - \langle \langle [m_\alpha v_\alpha^{(2)}(3\tau/2)]^2 / k_B \rangle_{(3),(2),(1)} \rangle_u \rangle_\alpha \quad (96)$$

or

$$\Delta T(3\tau/2) = \frac{T_0}{2} \left\langle e^{-b_\alpha \tau} \frac{\omega_\alpha^2}{\Omega_\alpha^2} \left[1 - \cos(2\Omega_\alpha \tau) - \frac{b_\alpha}{\Omega_\alpha} \sin(\Omega_\alpha \tau) + \frac{b_\alpha}{2\Omega_\alpha} \sin(2\Omega_\alpha \tau) \right] \right\rangle_\alpha. \quad (97)$$

For $b_\alpha = 0$ for all α , i.e., for oscillators without friction and fluctuating forces, Eq. (97) yields a τ -independent echo depth

$$\Delta T(3\tau/2) = \frac{T_0}{2} [1 - C_{T,T}(\tau)] \approx \frac{T_0}{2} \quad (98)$$

which reproduces the result (45) derived for the harmonic model for $\lambda_1 = \lambda_2 = 1$.

In the case $b_\alpha \neq 0$, holds⁴⁶

$$\frac{\langle m_\alpha x_\alpha(0) x_\alpha(2\tau) \rangle}{\langle m_\alpha x_\alpha^2 \rangle} = e^{-b_\alpha \tau} \left[\cos(2\Omega_\alpha \tau) + \frac{b_\alpha}{2\Omega_\alpha} \sin(2\Omega_\alpha \tau) \right]; \quad (99)$$

$$\frac{\langle m_\alpha v_\alpha(0) v_\alpha(2\tau) \rangle_\alpha}{\langle m_\alpha v_\alpha^2 \rangle} = e^{-b_\alpha \tau} \left[\cos(2\Omega_\alpha \tau) - \frac{b_\alpha}{2\Omega_\alpha} \sin(2\Omega_\alpha \tau) \right].$$

For $\tau \gg \tau_0$, both of the above quantities are small, such that $\langle b_\alpha / \Omega_\alpha \sin(\Omega_\alpha \tau) \rangle_\alpha$ and $\langle \cos(2\Omega_\alpha \tau) \pm b_\alpha / 2\Omega_\alpha \sin(2\Omega_\alpha \tau) \rangle_\alpha$ can be assumed to be negligible. Accordingly, we approximate Eq. (97)

$$\Delta T(3\tau/2) \approx \frac{T_0}{2} \left\langle e^{-b_\alpha \tau} \frac{\omega_\alpha^2}{\Omega_\alpha^2} \right\rangle_\alpha. \quad (100)$$

In the limit $b_\alpha \ll \omega_\alpha$ and choosing b_α the same constant b_0 for all α , follows

$$\Delta T(\tau) \approx \frac{T_0}{2} e^{-b_0 \tau}. \quad (101)$$

This result can be related to the phase diffusion model in Section VII. Comparing (101) and (78) for the CVRE, i.e., for $\lambda_1 = \lambda_2 = 1$, yields

$$b_0 = 3 \gamma_0 T_0. \quad (102)$$

5. Comparison with simulation results

Results for simulation of CVREs presented in Figs. 10, 11 demonstrate an exponential dependence of the echo depth on τ . The results also reveal that b_0 is proportional to temperature. Comparing Eq. (101) with the simulation results (cf. Fig. 10) one determines a b_0 value of 1.6 ps^{-1} at $T_0 = 290.55 \text{ K}$. The relaxation rate 1.6 ps^{-1} is much smaller than most protein frequencies.^{4,5} Hence, we conclude that protein modes are mainly underdamped. This result justifies the assumption (86).

There exist some earlier studies which determined the friction coefficients in proteins.⁴⁷ The friction coefficients measured in Ref. 47 for the atoms along two lysine chains of the protein RNase lie in the range $19\text{--}45 \text{ ps}^{-1}$, i.e., they are much higher than our present values. The discrepancy to our smaller number is not unexpected since the work in Ref. 47 measured the friction coefficients in Cartesian coordinates for single atom motion, whereas we calculated here the friction coefficients in the normal mode space. Many contributions to frictions and random forces in the Cartesian space are projected to become harmonic contributions in the normal mode space so that the friction coefficients of normal modes are expected to be much smaller than the ones calculated from a single atomic trajectory. As a matter of fact, it is observed in the simulation of an α -helical polypeptide with eleven residues of glycoporphin that the normal mode of the lowest frequency, $\omega_1 = 1.91 \text{ ps}^{-1}$, has a friction coefficient of 0.35 ps^{-1} .⁴⁴

IX. DISCUSSION

We have introduced in this paper a generalization of the so-called temperature quench echoes.^{24,28,29} Reassignments of atomic velocities at $t=0$ and at $t=\tau$, using two correlated sets of Maxwellian velocities, produce a temperature quench-type echo at $t=2\tau$ and a new echo at $t=\frac{3}{2}\tau$. The $\frac{3}{2}\tau$ -echo can be produced without any change in temperature in the system, i.e., it involves a mild perturbation. The new echo arises due to phase coherence and does not require amplitude modulation. The depth of the echoes is affected by phase relaxation and, therefore, provides information on the lifetime of coherent vibrations in proteins. The phase relaxation rate has been found to increase linearly with temperature. The dephasing times, at $T=300 \text{ K}$, measure about 500 fs to 1 ps , which is consistent with results reported in Refs. 17 and 22. This time scale is surprisingly long and establishes the relevance of protein normal modes. The echoes described can be monitored through the kinetic energy as well as through the potential energy of the system. The latter possibility revealed that the echoes are induced mainly by skeletal motions involving bond angle vibrations and, to a lesser degree, bond stretch vibrations.

The VRE method and the analysis of first results open an avenue for various future studies. One can relate, for ex-

ample, the phase relaxation in proteins to other physical properties which rely on anharmonic effects, e.g., to heat conduction as studied in Refs. 16 and 17. There exist numerous possibilities to extend the echo method presented. For example, one can apply multiple velocity reassignments using correlated velocity sets. In a first investigation we determined that, in case of seven CVRE-type assignments, the pure $\frac{3}{2}\tau$ -echo deepened and developed only a single co-echo, namely one at $t=2\tau$. This behaviour is distinct from that of multiple temperature quench echoes reported in Ref. 29.

One may involve only reassignments for a localized subset of atoms, e.g., atoms of a prosthetic group or substrate, to investigate how extended protein modes are.¹⁶ One may also explore correlations between the velocity sets (16) and (19) which differ from the simple correlation stated through (20), as discussed in Eq. (47). One might use velocity sets with weaker correlations than (7), or employ correlations which involve a spatial redirection, e.g., velocity sets with a correlation as expressed through (7), except that x -, and y -components in the set $\mathcal{V}^{(2)}$ are interchanged.

One may also alter velocities through the application of δ -forces $\{f_j \delta(t), f'_j \delta(t-\tau), j=1,2,\dots,3N\}$ where the random force strengths $\{f_j, f'_j, j=1,2,\dots,3N\}$ are correlated in a similar way as the VREs. One may also consider to assign instead harmonic forces $\{f_j \sin \omega t, j=1,2,\dots,3N\}$ with random strengths f_j , spatially correlated strengths f_j , e.g., $\langle f_j f_k \rangle \sim \exp(-|\vec{r}_j - \vec{r}_k|/r_0)$ where \vec{r}_j, \vec{r}_k denote the spatial position of atoms, or spatially homogenous f_j describing IR absorption.⁹

An interesting alternative to the use of Cartesian velocities in Eqs. (4) and (6) would be the use of velocities along internal coordinates. Such choice would be particularly interesting for a study of selective excitations through echoes, both spatially selective and selective for types of internal coordinates. Such assignment could also avoid the problems associated with a drift of the transformation $\mathbf{S}(t)$ defined in Eqs. (14) and (15).

A major conclusion of the present study stems from the difference in the decay times of $\frac{3}{2}\tau$ - and 2τ -echoes: we claim that this difference is due to a change in normal modes when a protein moves between conformational substates. These changes are accounted for by $g_\alpha(\tau, T)$ in Eq. (21). It would be of interest to determine $g_\alpha(\tau, T)$ directly from molecular dynamics simulations. This is feasible through evaluation of the $3N \times 3N$ position, velocity, and force correlation matrices $M_{jk}(t_n) = \langle h_j(t) h_k(0) \rangle$ where $h_j(t)$ represents the Cartesian components of position, velocity or force for all atoms of a protein at times t_0, t_1, \dots . Diagonalization of these matrices yields quasi-harmonic modes which can be used to determine $g_\alpha(\tau, T)$ or the change in correlation of the velocity sets (16) and (17).⁴⁸ This quasi-harmonic description may actually also lead to an identification of the modes participating in the VRE.

A key question for future studies regards the biological relevance of the motions participating in echoes. One expects that these motions can differentiate between α -helical segments and β -sheets. This invites a systematic study of proteins with distinct α -helical and β -sheet domains. A first exploration of echoes of denatured proteins revealed that

echo depths were little affected by the denaturation, i.e., the motions depend mainly on secondary structure. The modes observed through echoes might be coupled, for example, to electron transfer.^{49,50} They might also be functionally important being involved in sonic speed allosteric coupling between different sites in a protein as suggested in Ref. 18. The modes may also be essential in signal transfer, e.g., in case of membrane proteins with long α -helical segments.^{51,52}

ACKNOWLEDGMENTS

We thank M. Karplus, O. Becker, S. Tzonev and M. Balsera for valuable discussions and encouraging comments. This work has been supported by the National Institute of Health (grant P41RRO5969). Some of the simulations were carried out on a Connection Machine CM-200 operated by the National Center for Supercomputing Applications at the University of Illinois.

- ¹N. W. Ashcroft and N. D. Mermin, *Solid State Physics* (Saunders, Philadelphia, 1976).
- ²R. G. Lerner and G. L. Trigg, *Encyclopedia of Physics*, 2nd ed. (VCH, New York, 1990).
- ³T. Noguti and N. Gō, *Nature* **296**, 776 (1982).
- ⁴B. R. Brooks and M. Karplus, *Proc. Natl. Acad. Sci. U.S.A.* **80**, 6571 (1983).
- ⁵M. Levitt, C. Sander, and P. S. Stern, *J. Mol. Biol.* **181**, 423 (1985).
- ⁶N. Gō, T. Noguti, and T. Nishikawa, *Proc. Natl. Acad. Sci. U.S.A.* **80**, 3696 (1983).
- ⁷R. M. Levy, A. R. Srinivasan, W. K. Olson, and J. A. McCammon, *Biopolymers* **23**, 1099 (1984).
- ⁸R. M. Levy, O. de la Luz Rojas, and R. A. Friesner, *J. Phys. Chem.* **88**, 4233 (1984).
- ⁹E. Henry, W. Eaton, and R. Hochstrasser, *Proc. Natl. Acad. Sci. U.S.A.* **83**, 8982 (1986).
- ¹⁰J. Gibrat and N. Gō, *Proteins: Struct. Funct. Genet.* **8**, 258 (1990).
- ¹¹B. R. Brooks and M. Karplus, *Proc. Natl. Acad. Sci. U.S.A.* **82**, 4995 (1985).
- ¹²J. Smith, S. Cusack, U. Pezzeca, B. Brooks, and M. Karplus, *J. Chem. Phys.* **85**, 3636 (1986).
- ¹³J. Smith, S. Cusack, B. Tidor, and M. Karplus, *J. Chem. Phys.* **93**, 2974 (1990).
- ¹⁴S. Cusack and W. Doster, *Biophys. J.* **58**, 243 (1990).
- ¹⁵J. S. Ahn, Y. Kanematsu, M. Enomoto, and T. Kushida, *Chem. Phys. Lett.* **215**, 336 (1993).
- ¹⁶T. Lian, B. Locke, Y. Kholodenko, and R. M. Hochstrasser, *J. Phys. Chem.* **98**, 11648 (1994).
- ¹⁷R. Alden, M. Schneebeck, M. Ondrias, S. Courtney, and J. Friedman, *J. Raman Spectrosc.* **23**, 569 (1992).
- ¹⁸R. D. Miller, *Acc. Chem. Res.* **27**, 145 (1994).
- ¹⁹G. Zhang and T. Schlick, *J. Comput. Chem.* **14**, 1212 (1993).
- ²⁰G. Zhang and T. Schlick, *J. Chem. Phys.* **101**, 4995 (1994).
- ²¹J. Durup, *J. Phys. Chem.* **95**, 1817 (1991).
- ²²R. M. Levy, D. Perahia, and M. Karplus, *Proc. Natl. Acad. Sci. U.S.A.* **79**, 1346 (1982).
- ²³B. Mao, M. R. Pear, J. A. McCammon, and S. H. Northrup, *Biopolymers* **21**, 1979 (1982).
- ²⁴G. S. Grest, S. R. Nagel, and A. Rahman, *Solid State Commun.* **36**, 875 (1980).
- ²⁵G. S. Grest, S. R. Nagel, A. Rahman, and T. W. Witten, Jr., *J. Chem. Phys.* **74**, 3532 (1981).
- ²⁶S. R. Nagel, A. Rahman, and G. S. Grest, *Phys. Rev. Lett.* **47**, 1665 (1981).
- ²⁷S. R. Nagel, G. S. Grest, and A. Rahman, *Physics Today* **October**, 24–32 (1983).
- ²⁸O. M. Becker and M. Karplus, *Phys. Rev. Lett.* **70**, 3514 (1993).
- ²⁹D. Xu, K. Schulten, O. Becker, and M. Karplus, *J. Chem. Phys.* **103**, 3112 (1995).
- ³⁰J. Deisenhofer and W. Steigemann, *Acta Crystallogr. Sect. B* **31**, 238 (1975).
- ³¹J. A. Board, Jr., J. W. Causey, J. F. Leathrum, Jr., A. Windemuth, and K. Schulten, *Chem. Phys. Lett.* **198**, 89 (1992).
- ³²A. Windemuth and K. Schulten, *Mol. Sim.* **5**, 353 (1991).
- ³³B. R. Brooks, R. E. Bruccoleri, B. D. Olafson, D. J. States, S. Swaminathan, and M. Karplus, *J. Comput. Chem.* **4**, 187 (1983).
- ³⁴H. J. C. Berendsen, J. P. M. Postma, W. F. van Gunsteren, and A. DiNola, *J. Chem. Phys.* **81**, 3684 (1984).
- ³⁵A. T. Brünger, X-PLOR, Version 3.1, A System for X-ray Crystallography and NMR, The Howard Hughes Medical Institute and Department of Molecular Biophysics and Biochemistry, Yale University, 1992.
- ³⁶S. Lifson and P. S. Stern, *J. Chem. Phys.* **77**, 4542 (1982).
- ³⁷H. Frauenfelder, F. Parak, and R. Young, *Annu. Rev. Biophys. Biophys. Chem.* **17**, 451 (1988).
- ³⁸L. Rayleigh, *Scientific Papers* (Cambridge University Press, Cambridge, England, 1899–1920), Vol. I, p. 491.
- ³⁹S. A. Rice, *J. Chem. Phys.* **33**, 1376 (1960).
- ⁴⁰S. Wolfram, *Mathematica, A System for Doing Mathematics by Computer*, 2nd ed. (Addison-Wesley, New York, 1991).
- ⁴¹S. R. Nagel, G. S. Grest, and A. Rahman, *Phys. Rev. Lett.* **53**, 368 (1984).
- ⁴²C. W. Gardiner, *Handbook of Stochastic Methods for Physics, Chemistry, and the Natural Sciences* (Springer, New York, 1985).
- ⁴³B. Cartling, *J. Chem. Phys.* **91**, 427 (1989).
- ⁴⁴B. Cartling, *J. Chem. Phys.* **94**, 6203 (1991).
- ⁴⁵S. Chandrasekhar, *Rev. Mod. Phys.* **15**, 1 (1993).
- ⁴⁶M. C. Wang and G. E. Uhlenbeck, *Rev. Mod. Phys.* **17**, 323 (1945).
- ⁴⁷W. Nadler, A. Brünger, K. Schulten, and M. Karplus, *Proc. Natl. Acad. Sci. U.S.A.* **84**, 7933 (1987).
- ⁴⁸M. Balsera, Y. Oono, and K. Schulten (in preparation).
- ⁴⁹D. Xu and K. Schulten, *NATO ASI Series A: Life Sciences*, NATO ASI Series A: Life Sciences (Plenum Press, New York, 1992), pp. 310–312.
- ⁵⁰D. Xu and K. Schulten, *Chem. Phys.* **182**, 91 (1994).
- ⁵¹E. A. Barnard, *TIBS* **17**, 368 (1992).
- ⁵²A. Aderem, *TIBS* **17**, 438 (1992).